Molecular Cancer

RESEARCH

Open Access

# LMTK3 regulation of EV biogenesis and cargo sorting promotes tumour growth by reducing monocyte infiltration and driving pro-tumourigenic macrophage polarisation in breast cancer

Mark Samuels[1,2], Christos Karakostas[3], Simoni Besta[1,2], Andrea Lauer Betrán[2], Katerina Tsilingiri[3], Charlotte Turner[2], Reza Shirazi Nia[1], Niloufar Poudine[1], Richard Goodyear[4], William Jones[2], Apostolos Klinakis[3] and Georgios Giamas[1,2*]

## Abstract

**Background** Lemur Tail Kinase 3 (LMTK3) promotes cell proliferation, invasiveness and therapy resistance, and its expression correlates with poor survival in several different malignancies, including breast cancer. Crosstalk through extracellular vesicles (EVs) is an increasingly appreciated mechanism of cell communication within the tumour immune microenvironment, which contributes to different aspects of cancer progression and plays a pivotal role in shaping tumour fate.

**Methods** Nanoparticle tracking analysis and transmission electron microscopy were used to study the effects of LMTK3 on EV size, while single particle interferometry allowed us to examine LMTK3-dependent effects on the subpopulation distribution of EVs. Quantitative mass spectrometry was used to profile LMTK3-dependent proteomics changes in breast cancer-derived EVs. Bioinformatics analysis of clinical data along with in vitro and cell-based assays were implemented to explore the effects of LMTK3-dependent EV protein cargo on the tumour immune microenvironment. To elucidate the mechanism through which LMTK3 impacts endosomal trafficking and regulates EV biogenesis, we used a variety of approaches, including in vitro kinase assays, confocal and electron microscopy, as well as in vivo subcutaneous and orthotopic breast cancer mouse models.

**Results** Here, we report that LMTK3 increases the average size of EVs, modulates immunoregulatory EV proteomic cargo and alters the subpopulation distribution of EVs released by breast cancer cells. Mechanistically, we provide evidence that LMTK3 phosphorylates Rab7, a key regulator of multivesicular body (MVB) trafficking, thereby reducing the fusion of MVBs with lysosomes and subsequent degradation of intralumenal vesicles, resulting in altered EV release. Moreover, LMTK3 causes increased packaging of phosphoserine aminotransferase 1 (PSAT1) in EVs, leading to a paracrine upregulation of phosphoglycerate dehydrogenase (PHGDH) in monocytes when these EVs are taken up. PSAT1 and PHGDH play key roles in the serine biosynthesis pathway, which is closely linked to cancer progression and regulation of monocyte behaviour. LMTK3 EV-induced elevated PHGDH expression in monocytes reduces their

*Correspondence:
Georgios Giamas
g.giamas@sussex.ac.uk; georgios.giamas@zcmu.edu.cn
Full list of author information is available at the end of the article

© The Author(s) 2025. **Open Access** This article is licensed under a Creative Commons Attribution-NonCommercial-NoDerivatives 4.0 International License, which permits any non-commercial use, sharing, distribution and reproduction in any medium or format, as long as you give appropriate credit to the original author(s) and the source, provide a link to the Creative Commons licence, and indicate if you modified the licensed material. You do not have permission under this licence to share adapted material derived from this article or parts of it. The images or other third party material in this article are included in the article's Creative Commons licence, unless indicated otherwise in a credit line to the material. If material is not included in the article's Creative Commons licence and your intended use is not permitted by statutory regulation or exceeds the permitted use, you will need to obtain permission directly from the copyright holder. To view a copy of this licence, visit http://creativecommons.org/licenses/by-nc-nd/4.0/.

infiltration into breast cancer 3D spheroids and in vivo breast cancer mouse models. Furthermore, these infiltrating monocytes preferentially differentiate into pro-tumourigenic M2-like macrophages. Additional breast cancer mouse studies highlight the contribution of LMTK3-dependent EVs in the observed immunosuppressive macrophage phenotype. Finally, in vitro experiments show that pharmacological inhibition of LMTK3 reverses the pro-tumourigenic and immunomodulatory effects mediated by EVs derived from LMTK3 overexpressing cells.

**Conclusion** Overall, this study advances our knowledge on the mechanisms of EV biogenesis and highlights a novel oncogenic role of LMTK3 in the breast TME, further supporting it as a target for cancer therapy.

**Keywords** LMTK3, Rab7, Extracellular Vesicles, Breast Cancer, Monocytes, Macrophages, Tumour Microenvironment

## Introduction

Lemur tail kinase 3 (LMTK3) is a serine/threonine protein kinase with critical roles in different malignancies, including breast cancer (BC) where its upregulation drives key cellular and oncogenic processes, such as estrogen receptor α (ERα) transcription and stabilisation, chromatin remodelling, resistance to chemo- and endocrine- therapies, invasion and metastasis [1–7]. Through its regulation of these oncogenic processes, LMTK3 upregulation in BC strongly correlates with poorer survival, higher tumour grade and more advanced disease, highlighting its association with more aggressive cancers [8]. Consequently, it is not surprising that LMTK3 has emerged as a promising target for cancer therapy.

LMTK3 belongs to the LMTK family of kinases. Interestingly, both LMTK1 and LMTK2 isoforms have been implicated in endosomal trafficking [9], while depletion of LMTK2 can lead to impaired recycling of the transferrin receptor and result in swollen endosomes [10]. Endosomal trafficking is controlled by Rab proteins, a large family of small GTPases regulating the movement of intracellular cargo between organelles [11]. Amongst them, Rab7a is particularly important for the maturation of early to late endosomes, which is crucial for the sorting and degradation of cellular cargo and the formation of multivesicular bodies (MVBs) [12, 13]. MVBs are important structures in extracellular vesicle (EV) biogenesis, as the membrane of the late endosomes can undergo inward budding forming intraluminal vesicles (ILVs). The MVBs can then fuse with the plasma membrane, releasing the ILVs as exosomes, a subtype of EV specifically arising through the endosomal pathway [14]. The regulation of endosomal trafficking by LMTKs therefore suggests the kinases may have a role in the regulation of EV biogenesis. EVs are lipid bilayer-delimited particles naturally released from cells and exosomes are a subtype of EV of endosomal origin. In disease, EVs have been proposed as useful candidates for biomarkers, as well as promising drug delivery systems for therapeutic agents. However, interestingly, EVs also mediate intercellular communication by carrying proteins, nucleic acids, and other bioactive cargo, contributing to numerous physiological processes. In particular, EVs have gained significant recognition for their roles in immunity, inflammation and cancer progression through facilitating communication between cancer cells and immune cells [15].

Monocytes are short-lived mononuclear myeloid lineage cells that circulate in blood and have different subtypes (classical, non-classical and intermediate) that are involved in phagocytosis, migration, innate immune responses, cytokine secretion and antigen presentation [16, 17]. In BC, monocyte infiltration and expansion in the tumour microenvironment (TME) correlates with disease stage and tumour size [18–21]. After their recruitment into tumours, monocytes can differentiate into a heterogeneous population of macrophages, which, although oversimplified, can be broadly categorised as M1-like or M2-like subsets [22]. Pro-inflammatory (anti-tumourigenic) M1-like macrophages are key to immune response against bacteria and promote T helper 1 (Th1) T cell activity, while M2-like anti-inflammatory (pro-tumourigenic) macrophages contribute to wound healing and immunosuppression [23]. Macrophages are highly plastic cells and can alter their phenotype based on environmental cues. Although early BC features many M1-like macrophages that inhibit cancer growth through phagocytosis and secretion of tumour necrosis factor alpha (TNF-α) and reactive oxygen species (ROS), late-stage tumours are characterised by the presence of M2-like cells that suppress natural killer (NK) and T cells, and promote BC growth, metastasis, and survival [24].

Among the many processes governing macrophage polarisation is metabolic reprogramming, which is an important hallmark of cancer. Changes in serine biosynthesis in particular are linked to malignancies and elevated levels of 3-phosphoglycerate dehydrogenase (PHGDH), the first rate-limiting enzyme of the serine biosynthesis pathway, have been implicated in cancer progression. Moreover, in monocytes and macrophages, PHGDH has been reported to act as a key metabolic checkpoint of macrophage polarisation [25], with

increased PHGDH activity correlating with an anti-inflammatory M2-like phenotype, while inhibition of PHGDH promotes an M1-like pro-inflammatory macrophage state [26, 27]. Interestingly, a recent study found that Th2 cytokine, IL-4, and tumour-conditioned media lead to an upregulation of PHGDH in macrophages, promoting M2 polarisation. In addition, PHGDH ablation in vivo resulted in a shift of macrophages from M2 to M1 state, a reduction in the infiltration of tumour-associated macrophages (TAMs), as well as an enhanced anti-tumour T cell immunity. These findings show that targeting PHGDH can reverse the immunosuppressive phenotype by promoting an M1-like phenotype in macrophages [28].

Despite the wealth of knowledge on the roles of LMTK3 in cancer, the involvement of LMTK3 in immune modulation remains largely unexplored. A study on early onset colorectal cancer (CRC) showed that LMTK3 mutations positively correlate with tumour mutation burden, $CD8^+$ T cell and macrophage infiltration, as well as with a 'hot' immunophenotype [29]. Similarly, Wei et al. found that elevated LMTK3 levels in CRC associate with high immune scores and increased abundance of $CD4^+$ and $CD8^+$ T cells [30]. However, no study to date has explored the role of LMTK3 in immune infiltration in BC.

In this study, we identify Rab7, a key player in late endosomal trafficking, as a novel phosphorylation substrate of LMTK3, through which, LMTK3 modulates EV biogenesis, leading to the generation of larger EVs with distinct proteomic cargo. These enlarged EVs carry a unique set of proteins that can reshape the immune TME. We show in BC cells and in vivo models that exposure of monocytes to EVs derived from LMTK3-overexpressing cells promotes M2-like polarisation in macrophages. Furthermore, EVs from LMTK3 overexpressing cells reduce infiltration of monocytes into tumours by promoting PHGDH upregulation. Taken together, we present evidence of LMTK3's implication in EV biogenesis and its involvement in the development of an immunosuppressive TME.

## Materials and methods

### Cell lines and cell culture

T47D, MCF7, MDA-MB-231, THP-1 and HEK293T cells were obtained from American Type Culture Collection (ATCC). 4T1 cells were obtained from Wuhan Pricella Biotechnology Co., Ltd. MMTV-Neu mammary carcinoma cell lines were generated in Professor Klinakis' lab. Briefly, endpoint mammary tumours in transgenic MMTV-Neu mice were dissociated and sorted for CD24 + cells which were kept in culture as luminal tumour cells [31]. MDA-MB-231, MMTV-Neu and HEK293T cells were cultured in Dulbecco's Modified Eagle Medium (DMEM) (Sigma Aldrich, D6046-500ML) supplemented with 10% foetal bovine serum (FBS) (Sigma Aldrich, F7524-500ML) and 1% penicillin/streptomycin (P/S) (Sigma Aldrich, P4333-100ML), unless otherwise specified. T47D, 4T1 and THP-1 cells were cultured in Roswell Park Memorial Institute 1640 medium (RPMI-1640) (Sigma Aldrich, R5886-500ML) supplemented with 10% FBS and 1% P/S. The cells were maintained in a humidified incubator with 5% $CO_2$ at 37 °C and were routinely checked for mycoplasma contamination (Sigma Aldrich, MP0035). In experiments involving LMTK3 inhibition, C28 (MedChemExpress, HY-153896) was used at a final concentration of 10 µM, diluted in DMSO.

### Transfection and generation of stable cell lines

Overexpression of LMTK3 was achieved using the pCMV6-FLAG-LMTK3 plasmid encoding full-length LMTK3 (Origene, RC223140). Ectopic expression of the Rab7 mutants was achieved using site-directed mutagenesis of pCMV6-Rab7 vectors generated from mCherry-Rab7a-7, a gift from Michael Davidson (Addgene plasmid #55127). The empty pCMV6 vector (Origene, PS100001) was used as a control and the pCMV6 vector containing full length Rab7 (pCMV6-Rab7) was used for Rab7 overexpression. Rab7 knockout was achieved by cloning a Rab7-targeting sgRNA into the px459 vector using the primers: 5′-CACCGTTGCTGAAGGTTATCATCC-3′ forward (Fw), 5′-AAACGGATGATAACCTTCAGC AAC-3′ reverse (Rv). pSpCas9(BB)−2A-Puro (PX459) V2.0 was a gift from Feng Zhang (Addgene plasmid #62988) [32]. Following transfection with FuGENE® HD transfection reagent (Promega, E2311), the cells were selected with Geneticin (G418) (Sigma Aldrich, G8168-10ML) or Puromycin (Gibco, A11138-03) for one week, or until no viable cells remained in the non-transfected control group. Single cell clone populations were grown and used for the validation of successful protein expression through western blotting. PHGDH and PSAT1 overexpression were achieved using the lentivectors, pLJM5-PHGDH and pTRIPZ-PSAT1, a kind gift from Dr Katiuscia Bianchi.

### Preparation of conditioned media

Five million cells were seeded per flask in five T175 flasks in 20 mL complete growth media. Once 80% confluence was reached, cells were washed three times with 5 mL PBS. 15 mL serum-free media was then added to each flask and the cells were placed in an incubator for 24 h. The conditioned media was then collected and centrifuged at 2,000 ×g for 10 min at room temperature to remove cells and cell debris. The supernatant was

transferred to a new tube and either processed immediately or stored at −20 °C for future use for up to one month.

#### Extracellular vesicle separation

Centrifugation steps were performed using an Optima LE 80-k ultracentrifuge and a Type 70 Ti rotor. Conditioned media was distributed into four Beckman 25 × 89 mm polycarbonate tubes (Beckman, 355654) and centrifuged at 10,000 × g for 30 min at 4 °C to pellet cell debris and large EV-like particles. The supernatant was then transferred into four new tubes by syringing and filtering through a 0.2 µm filter. It was then centrifuged at 100,000 × g for 90 min at 4 °C to pellet EVs. To wash the EVs, the four EV pellets were resuspended in 1 mL PBS. The EVs were then combined in a new tube. The volume was made up to 10 mL with PBS and the samples were centrifuged again at 100,000 × g for 90 min at 4 °C. The supernatant was discarded by pouring and the pellet resuspended in 100 µL PBS and stored at −80 °C for up to three months.

#### Immunofluorescence

30,000 cells were plated on sterile coverslips in complete media in a 24-well plate. Once attached, cells were washed once and fixed in 4% paraformaldehyde in PBS for 10 min at room temperature. Cells were then permeabilised with 0.1% NP-40 for 15 min at room temperature. The cells were then blocked with 3% BSA in PBS for 30 min at room temperature and incubated with primary antibodies at 1:100 dilution, in a humidified chamber overnight at 4 °C. Following three washes with PBS, the cells were incubated with fluorophore-conjugated secondary antibodies at a 1:1000 dilution for 1 h at room temperature. The coverslips were then washed three times with PBS before they were mounted onto slides with ProLong Diamond Antifade mountant with DAPI. Cells were then imaged with the LSM880 confocal microscope.

#### Cell lysis and western blotting

Cells were lysed in radioimmunoprecipitation assay (RIPA) buffer (Sigma–Aldrich, R0278) containing protease inhibitors (Roche, 11697498001) and phosphatase inhibitors (Roche, 4906845001). Protein concentration was determined using the BCA assay. 50 µg (cell-based experiments) or 10 µg (EV-based experiments) of protein extract was mixed with 5× loading buffer and heated to 95 °C for 10 min. Samples were run on 4–12% gels (GenScript, M00653) and transferred onto nitrocellulose membranes (ThermoFisher Scientific, IB23001) using the iBlot 2 (ThermoFisher Scientific, IB21001). Primary antibodies were prepared at 1:1000 dilution, unless otherwise stated in the supplementary methods, and incubated overnight at 4 °C. Secondary antibodies (1:3000) were incubated with the membrane for 1 h at room temperature. Horseradish peroxidase (HRP)-conjugated anti-mouse (Cell Signaling Technology, 7076P2) or anti-rabbit (Cell Signaling Technology, 7074P2) were used as appropriate. Membranes were visualised with SuperSignal West Pico PLUS chemiluminescent substrate (ThermoFisher Scientific, 34577) and images were obtained using the UVP ChemStudio Imaging System (Analityk jena). Quantification was performed using ImageJ densitometry analysis where the intensity of the bands was normalised to the loading control and statistical significance was determined using Student's t test or one-way Analysis of Variance (ANOVA) as appropriate.

#### EGFR degradation assay

300,000 cells were plated per well in a 6-well plate in complete growth media. The following day, the media was replaced with serum-free media for 24 h. Cells were treated with 50 µg/mL cycloheximide for 1 h prior to EGF treatment. 100 ng/mL EGF was added, and samples were collected at 0, 30, 60, 120 and 180 min and subjected to western blotting.

#### Co-immunoprecipitation (co-IP)

Cells were lysed with a mild lysis buffer (10 mM Tris pH 7.5, 250 mM NaCl, 1% Triton X-100) to avoid protein–protein interaction disruption. The lysate was sonicated for three cycles, 20 s on and 30 s off in an ultrasonic homogeniser (Scientz, JY99-IIDN). 1,500 µg of cell lysates were used for each co-IP reaction. The lysates were incubated with 1:100 of FLAG antibody or mouse IgG isotype antibody for the immunoprecipitation of FLAG-LMTK3 and with 1:100 of Rab7 or rabbit IgG antibody for the immunoprecipitation of Rab7. The reactions were incubated overnight at 4 °C under rotation. The next day, 5 µL of Protein G magnetic beads (Thermo Scientific, 88847) for the mouse antibodies and Protein A magnetic beads (Thermo Scientific, 88845) for the rabbit antibodies were added to each reaction and incubated for 1 h at room temperature under rotation. Elution of the co-IP was performed by adding 40 µL of 3× SDS sample buffer (Cell Signaling, 7722) to the magnetic bead immunocomplex and the samples were incubated at 95 °C for 5 min. The eluates were then used for western blotting analysis.

#### Flow cytometry

PBMC derived macrophages were analysed by flow cytometry using the BD Accuri c6. 500,000 cells were centrifuged at 2,000 × g for 3 min and the supernatant was discarded. The cells were resuspended in 500 µL resuspension buffer (0.5% BSA in PBS) and blocked with Fc Receptor Blocking Solution (Biolegend, 422302) for 30

min. They were then stained with antibodies (1:20) for 1 h and propidium iodide (1:1000) for 10 min. A minimum of 10,000 cells were analysed per sample. Mouse-derived tumour cell suspensions were stained for 20 min, and data were acquired by BD FACS Celesta flow cytometer, using BD FACSDiva software. Cells were gated as singlets and live cells, according to FSC-A/FSC-H and FSC-A/SSC-A scatter plots. Following this, CD45 + cells were gated, and total macrophages were selected as the double-positive (CD11b + F4/80 +) population. The M1 macrophage population was selected as MHCII+CD206- and the M2 population as MHCII-CD206+. FACS analysis was performed using FlowJo software, and statistical analysis was performed with GraphPad Prism.

#### In vitro kinase assays

In vitro kinase assays using radiolabelled adenosine triphosphate (ATP) were carried out to assess Rab7 phosphorylation by LMTK3. Recombinant human Rab7 was incubated with baculovirus expressed LMTK3 kinase domain and [y-$^{32}$P]ATP for 60 min at 30 °C, unless otherwise specified. The reaction mixture was then separated by SDS-PAGE using a 4–20% acrylamide gel. The gel was then stained with Quick Coomassie (NeoBiotech, NB-45–00078) overnight and de-stained for 1 h in three changes of 1% glycerol. Gels were then dried for 2 h at 64 °C in a heated vacuum gel dryer (Cleaver Scientific). X-ray films (Scientific Laboratories Supplies, MOL7016) were added to the gels in an autoradiography cassette (Amersham Biosciences, RPN11649). After 24 h of exposure, films were developed using an ECOMAX x-ray film processor (Protec).

#### TEM imaging

Samples were visualised using the JEOL JEM1400-Plus (Jeol, Tokio, Japan) (120 kV, LaB6) microscope with a Gatan OneView 4 K camera. Images were taken at 2,000 ×, 10,000 ×, 12,000 ×and 30,000 ×magnification. For sample preparation, please refer to the supplementary methods.

#### Quantitative real-time PCR

Total RNA was extracted using the PureLink RNA mini kit (Invitrogen, 12183018A). cDNA was synthesised using the high-capacity cDNA reverse transcription kit (ThermoFisher Scientific, 4368814). Quantitative RT-PCR was performed using the Luna Universal qPCR Master Mix (NEB, M3003S) in a StepOne thermal cycler (Applied Biosystems). At least three biological and three technical replicates were performed per experiment. Glyceraldehyde 3-Phosphate Dehydrogenase (GAPDH) was used as an internal control. The following primers were used: GAPDH Fw 5'-TCGGAGTCAACGGATTTG-3', Rv 5'-CAACAATATCCACTTTACCAGAG-3', CD86 Fw 5'-AGTGAACAGACCAAGAAAAGAGAAA-3', Rv 5'-AGGTTGCCCAGGAACTTACAA-3', NOS2 Fw 5'-CAATGGCAACATCAGGTCGG-3', Rv 5'-GTGAATTCCACGTTGGCAGG-3', CD206 Fw 5'-TGCTACTGAACCCCCACAAC-3', Rv 5'-AACCAGAGAGGAACCCATTCG-3', TGFB1 Fw 5'-GGTGGAAACCCACAACGAAAT-3', Rv 5'-GAGCAACACGGGTTCAGGTA-3'.

#### Nanoparticle tracking analysis

The Nanosight NS300 was used to quantify EVs and measure their size. A 1 mL syringe and syringe pump were used to feed the EV suspension into the flow chamber of the Nanosight. 2–10 µL of EV suspension was diluted in 1000 µL PBS and loaded using a 1 mL syringe. A flow rate of 70 AU was used, and the camera setting was between 13 and 15. The tubes were washed with 2 mL PBS before and after each use to remove debris and the flow cell was washed in dd$H_2O$ prior to use. Five measurements of 60 s were taken per sample. The camera type was sCMOS and the laser type was Blue488.

#### Single particle interferometric reflectance imaging

The Unchained Labs Leprechaun was used for EV subpopulation analysis according to the manufacturer's instructions using the Leprechaun Exosome Human Tetraspanin Kit (Unchained Labs, 251–1044). Conditioned media from control and LMTK3 cells was diluted 1:4 with dilution buffer and 50 µL was added per chip. Chips were printed with anti-CD9, anti-CD63, anti-CD81 and anti-mouse IgG antibodies. The chips were incubated overnight and the following day, the chips were washed three times then incubated with primary antibodies for 1 h at room temperature. The chips were then washed three times with wash buffer then in deionised water then dried, imaged, and analysed with the Leprechaun.

#### PBMC and monocyte isolation

Blood from healthy volunteers was collected by venepuncture in four 4 mL EDTA tubes and transferred to a 50 mL falcon tube. The isolation of peripheral blood mononuclear cells (PBMCs) was performed as previously described following the Ficoll-Paque (Merck, Cytiva 17–1440-02) method [33]. Following this, monocytes were isolated by plastic adhesion [33]. Further monocyte population enrichment was performed using the PluriSpin Human Monocyte Enrichment solution (PluriSelect, 19–01001) according to the manufacturer's instructions.

#### Monocyte differentiation

THP-1 monocytes were differentiated into macrophages by incubation with 10 ng/mL of 12–0-tetradecanoylphorbol-13-acetate (PMA) (Sigma Aldrich, 524400) for 24 h. The media was then changed to normal complete media and the macrophages were allowed to rest for another 24 h.

#### 3D co-culture of monocytes and breast cancer cells

Tumour spheroids were cultured by coating each well of a 96-well plate with 100 µL of 1% agarose in PBS. 2,500 T47D or MDA-MB-231 cells were then added in 100 µL complete media and allowed to grow for 7 days. Monocytes were stained with green lipophilic tracer (Invitrogen, L7781). The monocytes were then added to spheroids with 2,500 monocytes per spheroid. After 24 h of co-culture, spheroids were washed three times in PBS and imaged using the JuLi stage live cell imaging microscope to assess infiltration. ImageJ was used to quantify the mean fluorescence within the spheroids. Briefly, spheroid fluorescence intensity was measured by drawing a region of interest around each spheroid and using the 'measure' function to obtain the mean fluorescence intensity. Background intensity was measured in a cell-free area and subtracted from the spheroid signal.

#### Extracellular vesicle uptake

CD63-RFP was expressed in T47D using pCT-CD63-RFP (System Biosciences, CYTO120R-PA-1) through lentiviral transduction and puromycin selection to generate a stable cell line. Cells were seeded in T175 flasks and EVs were collected as previously described. Monocytes were grown on coverslips in a 24-well plate and treated with different concentration of CD63-RFP EVs for 24 h. Following this, the plates were centrifuged at 300 ×g for 3 min and monocytes were fixed with 4% paraformaldehyde and mounted to the coverslips in 4',6-diamidino-2-phenylindole (DAPI)-containing ProLong Diamond Antifade mountant (ThermoFisher Scientific, P36962). They were then imaged with the LSM880 confocal microscope and EV uptake was assessed by measuring mean fluorescence intensity of cells using ImageJ.

#### Monocyte proliferation and viability assay

100,000 THP-1 monocytes were plated per well in a 24-well plate and treated with PBS or 10 µg/mL of control or LMTK3 EVs. At 24 h intervals, monocytes were counted, using the Countess automatic cell counter (ThermoFisher Scientific, C10281), and viability was measured using Trypan blue staining.

#### Immune cell infiltration

Data analysis of immune cell infiltration into tumours in clinical samples was performed using publicly available TCGA (The Cancer Genome Atlas) datasets [34–36], which were accessed through cBioPortal [37–39]. TIMER2.0 (Tumour Immune Estimation Resource version 2.0) [7] and xCell were used to obtain infiltration scores for immune cells in different tumours [40]. LMTK3 expression levels from RNA sequencing data were taken from cBioPortal and separated into four quartiles based on levels of LMTK3 and the first (Q1) and last (Q4) quartiles were compared to assess immune cell infiltration in tumours. For gene correlation analysis, mRNA levels for different M1 and M2 macrophage marker genes was then compared between these patient groups.

#### Animal models and sample processing

For the MMTV-Neu model, twelve male, Rag1-/- mice between 10 and 14 weeks old, obtained from Jackson labs (https://www.jax.org/strain/002216) were used in this experiment. MMTV-Neu control and LMTK3 overexpressing cells were used to grow subcutaneous or orthotopic tumours in the mice. Mice were grouped into two groups of six mice each, one for control and one for LMTK3 cells. $2\times 10^6$ cells in 100 µL DMEM/Matrigel mix (in 3:1 ratio) were injected in each murine flank for subcutaneous implantation or into the mammary fat pad for orthotopic implantation. From the day of injection (Day 0), mice were monitored for tumour growth twice a week, and tumour size was measured using a calliper.

For the 4T1 mouse model, SPF grade female BALB/c mice aged 6–8 weeks were purchased from Shanghai SLAC Experimental Animal Co., Ltd. (Shanghai, China). 4T1 cells were used to grow subcutaneous tumours in the right flanks of animals by injection of $5\times 10^5$ cells in 100 µL DMEM/Matrigel mix (in 1:1 ratio). Tumours were measured with a calliper and mice were injected with 50 µg EV protein/mouse in 50 µL PBS intratumourally three times per week.

#### Tumour isolation

All mice were sacrificed on day 32 (MMTV-Neu subcutaneous), day 23 (MMTV-Neu orthotopic) or day 29 (4T1) and tumours were excised for enzymatic digestion. Additionally, tumour biopsies were stored at −80 °C from each tumour, as well as tumour slices for paraffin embedding. Part of the tumours was cut and put in dissociation buffer, composed of 1 mg/mL Collagenase D (Roche, 11088858001) and 1 mg/mL Dispase (Sigma-Aldrich, D4693-1G) in DMEM F12 medium for 45 min. Once enzymatically dissociated, a single cell suspension was obtained after mechanical dissociation and passing through 70 µm cell strainer. The resulting mixture was

centrifuged at 400 ×g for 5 min. Red blood cells were lysed using ACK lysis buffer for 10 min, and RBC-free cell suspension was obtained to be used for flow cytometry. IHC was performed as described in the supplementary methods.

### Statistical analyses

Unless otherwise specified, data analysis was carried out using GraphPad Prism 9. Statistical tests were used depending on the experimental design as appropriate. Experiments were performed in triplicate unless otherwise stated. Column and line graphs show mean ± standard error of the mean (SEM) unless otherwise stated. Statistical significance was assessed using Student's t-test for comparison between two groups and one-way ANOVA followed by Tukey's multiple comparison test for multiple groups. A $p$-value < 0.05 was considered statistically significant.

For microscopy experiments where the size of structures is given, ImageJ was used. A line was drawn across the longest axis of each structure and the 'measure' function was used to determine the diameter.

### Data availability

The proteomics datasets generated in this study are both provided as supplementary tables S1 and S2.

## Results

### LMTK3 increases the size and regulates the proteomic cargo of EVs released by breast cancer cells

Considering the involvement of LMTK1 and LMTK2 in the endocytic pathway and the structural similarity between LMTK isoforms, we hypothesised that LMTK3 may also play a role in this fundamental process, as well as in EV biogenesis. To explore this, we initially generated a panel of BC cell lines (T47D, MCF7, and MDA-MB-231) stably overexpressing LMTK3 to explore how LMTK3 abundance impacts EVs. Western blotting confirmed the successful overexpression of LMTK3 (Fig. 1a). As previously reported, both bands represent full-length LMTK3, which may be subject to post-translational modifications [1]. Following collection of conditioned media, we used differential ultracentrifugation (DUC) to separate EVs, then validated the enrichment of EVs according to the minimal information for studies of extracellular vesicles (MISEV) guidelines [41] (Fig. 1b). Nanoparticle tracking analysis (NTA) was employed to determine particle size distribution and concentration (Fig. 1c-d). The analysis showed a significant increase in average EV size in all LMTK3-overexpressing BC cell lines (Fig. 1c), although, the EV concentration was not significantly altered (Fig. 1d). Furthermore, LMTK3 inhibition following treatment with C28 caused a decrease in average EV size without altering EV concentration. This suggests that LMTK3 affects an essential aspect of EV biogenesis without altering the quantity of EVs produced. Particle size distributions across the BC cell lines displayed the expected pattern, with a mode of ~ 100 nm and a right-skewed distribution (Figure S1a-c). LMTK3 overexpression increased the average diameter of EVs by approximately 20–30%, translating into a significant increase in EVs volume. The increase in EVs size was confirmed by an orthogonal measurement using transmission electron microscopy (TEM) (Fig. 1e-h).

Given the impact of LMTK3 on EV size, we next investigated whether LMTK3 can influence the proteomic cargo of BC cell-derived EVs. Tandem mass tag (TMT)-based mass spectrometry revealed substantial alterations in the protein content of EVs secreted by LMTK3-overexpressing BC cells (LMTK3 EVs) compared to control cells (Fig. 1i, Table S1). Interestingly, LMTK3 protein was also detected within the EVs following its overexpression.

(See figure on next page.)

**Fig. 1** Overexpression of LMTK3 increases average EV size, alters EV protein cargo, and changes the EV subpopulation distribution. **a**. Western blot for LMTK3 in LMTK3-overexpressing cells compared to control (pCMV6 empty vector) cells. GAPDH is shown as a loading control ($n = 3$). **b**. Western blot of cell lysate and EV fractions showing enrichment of the EV markers, CD9 and CD81, presence of HSP70 and depletion of GM130 in EVs compared to cell lysates ($n = 3$). **c**. Summary data showing mean EV size. **d**. NTA showing concentration of EVs. **e–g**. Representative transmission electron micrographs showing EVs from control and LMTK3-overexpressing breast cancer cells. Scale bars = 500 nm (12,000 x) and 100 nm (30,000 x). **h**. Quantification of (**e–g**). 500 EVs were measured for each condition. A representative distribution of EV size is shown. Median is shown with a solid line, and quartiles are shown with dotted lines. **i**. Proteomic analysis of EVs from control and T47D LMTK3-overexpressing cells. Volcano plot showing EV protein cargo changes as $\log_2$(fold change) of LMTK3 EVs/Control EVs. Significantly upregulated hits are shown in red and downregulated hits in blue (Welch's t test, $p < 0.05$). **j**,**k**. Western blotting of T47D (**j**) and MDA-MB-231 (**k**) cell lysate and EV fractions for control (Ct) and LMTK3-overexpressing cells. PSAT1, LDHB, CD63 and TSG101 were validated as hits from the proteomics analysis. CD9 and HSP70 were used as positive EV markers. GM130 was used as a negative EV marker ($n = 3$). **l**. Quantification of PSAT1 and LDHB levels in LMTK3 EVs relative to control EVs compared to HSP70. **m**. Quantification of CD63 and TSG101 levels in EVs relative to control EVs compared to HSP70. **n**. EV diameter for control and LMTK3 cells as measured by SP-IRIS. An increase in EV size is seen when LMTK3 is overexpressed for all three capture antibodies. **o**. The percentage abundance of particles positive for CD63, CD81 and CD9. CD63 positive particles were downregulated when LMTK3 was overexpressed. Graphs show the mean ± SEM of three independent experiments (*$p < 0.05$, **$p < 0.01$, ***$p < 0.001$, ****$p < 0.0001$; two-tailed unpaired Student's t-test) (**c**,**d**,**l**,**m**,**n**,**o**)

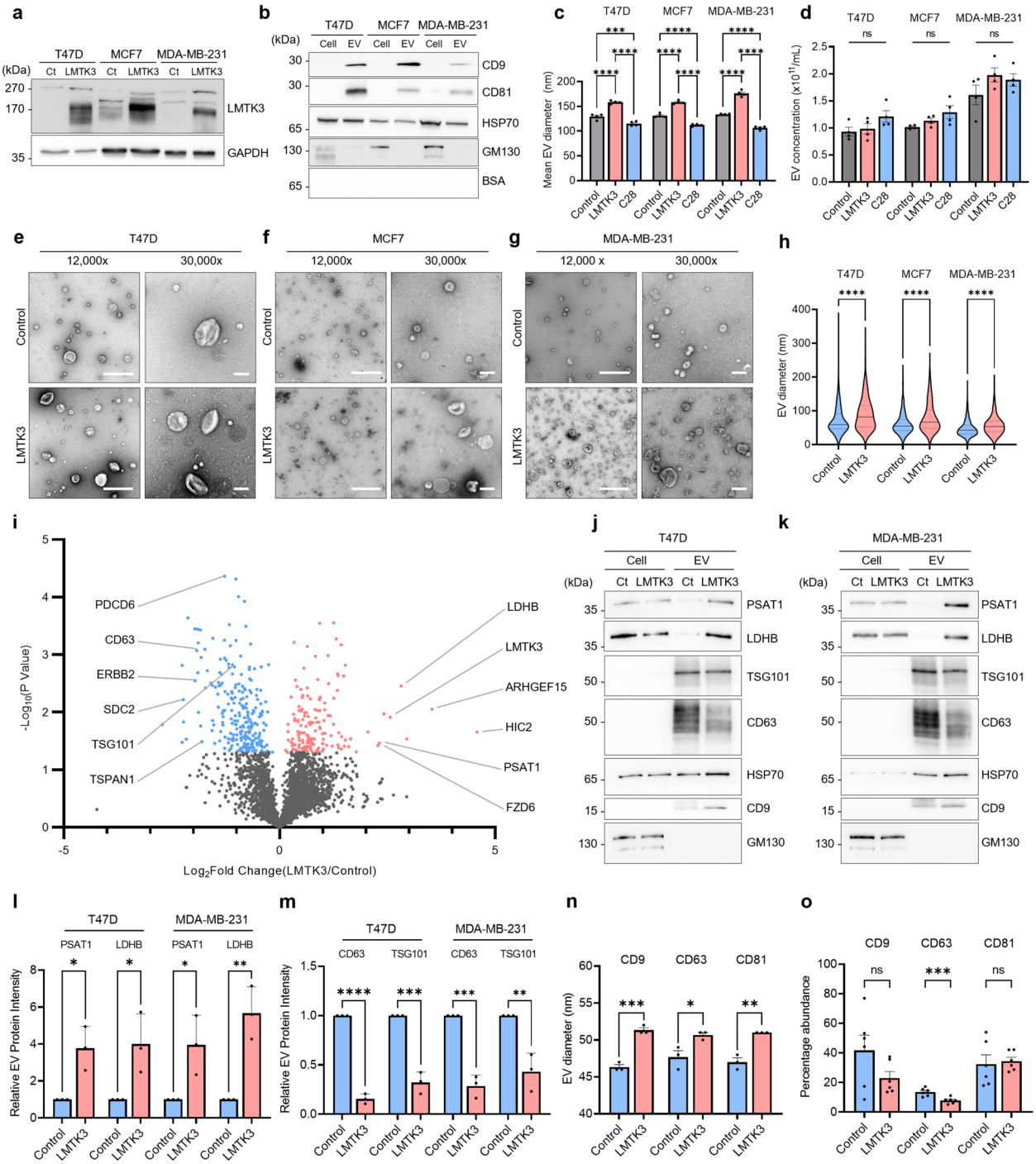


**Fig. 1** (See legend on previous page.)

Gene ontology (GO) pathway enrichment analysis highlighted significant upregulation of proteins associated with amino acids, endocytosis, Wnt and ERBB signalling, and other biological and cellular processes. Pathway analysis of the data indicate that LMTK3 EVs may play a functional role in modulating the TME via different mechanisms and signalling pathways (Figure S1d) [42]. Western blotting was used to validate different EV cargo proteins, including phosphoserine aminotransferase 1 (PSAT1) and lactate dehydrogenase B (LDHB) that were identified through our proteomics approach. These key metabolic enzymes, previously reported to be implicated in cancer

progression [43–45], were upregulated in the EVs secreted by LMTK3 overexpressing cells, while their total cellular levels remained unchanged, suggesting that LMTK3 selectively enhances their incorporation into EVs rather than regulating their cellular expression (Fig. 1j-m). Interestingly, several key components of exosome biogenesis were downregulated in EVs when LMTK3 was overexpressed, including syndecan-2 (SDC2), tumour suppressor gene 101 (TSG101) and tetraspanins (CD63 and TSPAN14), which further points to a role of LMTK3 in regulating EV biogenesis. Of these, CD63 and TSG101 were further validated as downregulated in LMTK3 overexpressing cell-derived EVs through western blotting (Fig. 1j-m).

EVs are heterogeneous in size, biogenesis, and function [46, 47]. To determine whether LMTK3 influences specific EV subpopulations, single-particle analysis was performed using the Unchained Labs Leprechaun® instrument, which employs single particle interferometric reflectance imaging sensor (SP-IRIS) technology to quantify surface EV markers [48]. EVs were immunocaptured with the tetraspanins CD9, CD63 and CD81, then immunolabelled with fluorescent antibodies against these proteins. The results showed a significant reduction in CD63-positive particles in LMTK3-overexpressing cells, suggesting a disruption in the tetraspanin-dependent exosome biogenesis pathway. This reduction aligns with the proteomics findings showing lower CD63 levels in LMTK3-derived EVs (Fig. 1n-o).

Taken together, using various experimental approaches, we demonstrated that LMTK3 upregulation in BC results in the formation of larger EVs with distinct protein cargo and changes to EV subpopulations, strongly suggesting a role for LMTK3 in EV biogenesis.

### LMTK3 regulates EV biogenesis and EV cargo loading by phosphorylating Rab7 at Ser72

Next, we investigated the possibility that LMTK3 regulates EV biogenesis through protein phosphorylation. To explore this hypothesis, we analysed previously published phosphoproteomics data [7] to identify prospective LMTK3 substrates involved in EV biogenesis. Our focus laid on Rab7 (Ser72), a small GTPase with key roles in MVB maturation and exosome release.

Previous studies have shown LMTK3 to co-localise with endosomal and Golgi markers in neurons, where it is involved in the endocytic trafficking of N-methyl D-aspartate (NMDA) receptors, while in BC cells, it is predicted to localise to the Golgi apparatus and early endosomes [49]. Rab7 is mainly detected in late endosomes (MVBs), which are the subcellular structures where exosomes are generated through the formation of ILVs and then released through fusion with the plasma membrane. To assess the prospective co-localisation between LMTK3 and Rab7, confocal microscopy was used. Following immunofluorescence staining, our analysis showed overlapping localisation between LMTK3 and Rab7, confirming that LMTK3 is present in late endosomes (Fig. 2a-b). Furthermore, co-immunoprecipitation assays using antibodies for FLAG-LMTK3 or Rab7 also confirmed the interaction between LMTK3 and Rab7 (Fig. 2c).

To investigate whether Rab7 mediates the observed LMTK3-dependent changes in EV biogenesis, we first assessed Rab7 phosphorylation at Ser72 in LMTK3-overexpressing cells. Western blotting confirmed that LMTK3 upregulation increases Rab7 phosphorylation without significantly altering Rab7 protein levels

(See figure on next page.)

**Fig. 2** LMTK3 directly phosphorylates Rab7 at Ser72. **a**. Immunofluorescence images of LMTK3 co-localisation with Rab7 in T47D and MDA-MB-231 cells. Scale bars = 10 µm and 1 µm (zoom). Images were taken with the LSM880 with Airyscan and a 63 × objective lens. **b**. Graph showing mean Pearson's correlation coefficient (r) for co-localisation between LMTK3 and Rab7 ($n = 50$ cells). **c**. Co-immunoprecipitation western blot showing interaction between LMTK3 and Rab7 in T47D LMTK3 cells. IgG is used as a negative control. Anti-FLAG (top) or anti-Rab7 (bottom) antibody was used to capture FLAG-LMTK3 and Rab7 respectively from cell lysates ($n = 3$). **d**. Western blot showing overexpression of LMTK3 leads to an increase in phospho Rab7 (serine 72). Tubulin was used as a loading control (n = 3). **e**. Quantification of intensity of pRab7/Rab7 in T47D and MDA-MB-231. Graphs show the mean ± SEM of three independent experiments (*$p < 0.05$, **$p < 0.01$; two-tailed unpaired Student's t-test). **f.** Western blot showing a decrease in Rab7 Ser72 phosphorylation following LMTK3 inhibition by C28. Tubulin is shown as a loading control ($n = 3$). **g**. Quantification of intensity of pRab7/Rab7 in T47D and MDA-MB-231. **h**. Western blot showing overexpression of LMTK3 in C28-treated cells restores Rab7 phosphorylation, showing specificity of C28 ($n = 3$). **i**. Quantification of (**h**). **j**. In vitro kinase assay of Rab7 and HSP27 (positive control) as substrates. An autoradiogram was produced to show phosphorylated proteins. 1 µM C28 was used to inhibit LMTK3 kinase activity. **k**. Western blot showing Rab7 phosphorylation by LMTK3 at Ser72. Following an in vitro kinase assay, proteins were separated by SDS PAGE. Western blot for phosphorylated Rab7 (Ser72) is presented ($n = 3$). **l**. Western blot showing overexpression of Rab7 mutant constructs in T47D and MDA-MB-231. Tubulin was used as a loading control ($n = 3$). **m**. Nanoparticle tracking analysis showing Rab7 S72E overexpression results in an increase in average EV size in T47D and MDA-MB-231 cells. **n**. Nanoparticle tracking analysis showing concentration of EVs from Rab7 mutant T47D and MDA-MB-231 cells. **o**,**p**. EVs were collected from the Rab7 mutant cell lines. Cell lysates and EVs were subjected to SDS-PAGE followed by western blotting. Figure showing a representative western blot showing PSAT1 levels in Rab7 mutant T47D (**o**) and MDA-MB-231 (**p**) cells. GM130 was used as a cellular marker and a negative EV marker. HSP70 and CD9 were used as positive EV markers ($n = 3$). **q**. Quantification of (**o**,**p**). Graphs show the mean ± SEM of at least three independent experiments (*$p < 0.05$, **$p < 0.01$, ***$p < 0.001$, ****$p < 0.0001$; one-way ANOVA, followed by Tukey's multiple comparisons test)

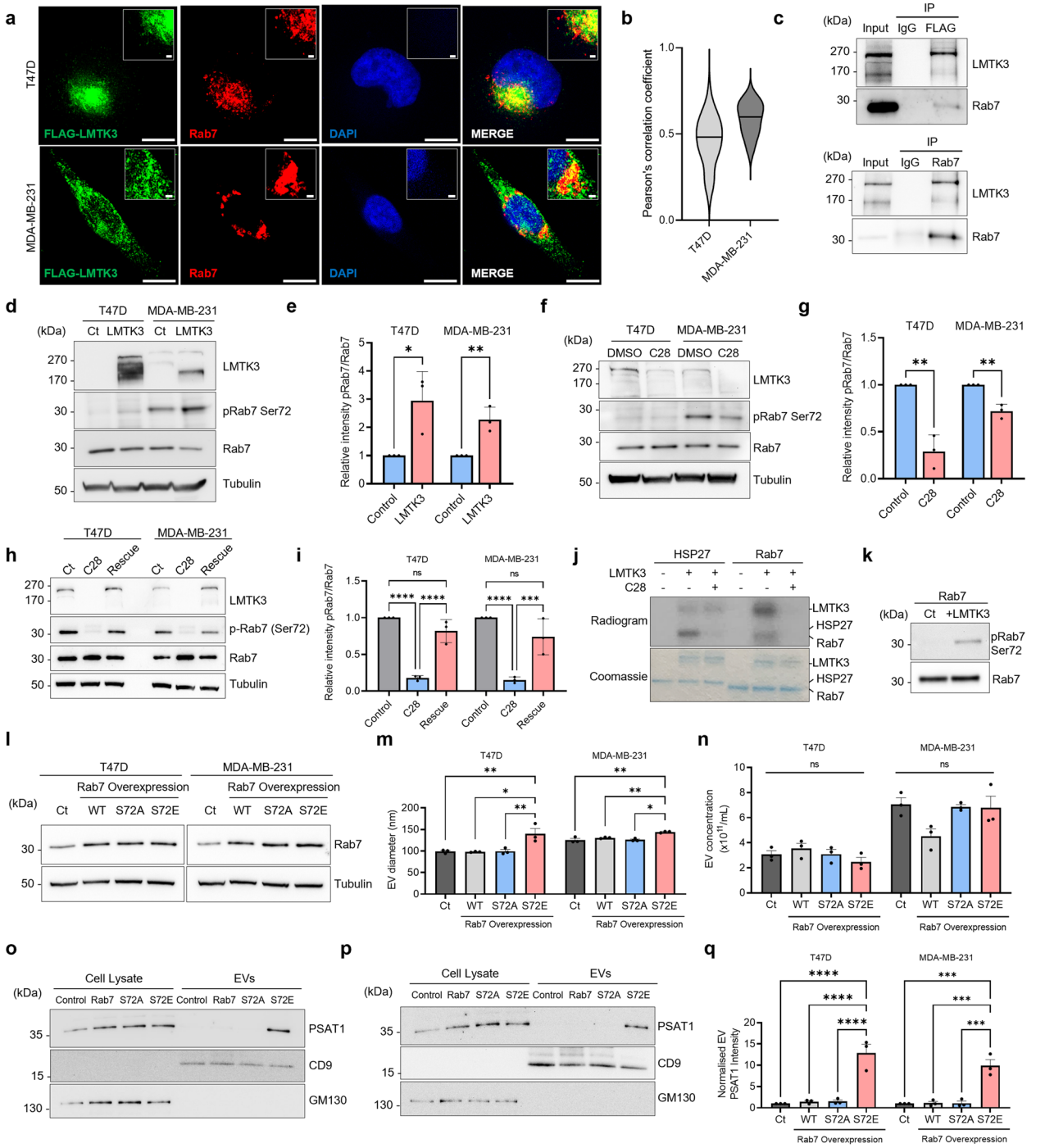


**Fig. 2** (See legend on previous page.)

(Fig. 2d-e). Furthermore, inhibition of LMTK3 using the selective LMTK3 inhibitor (C28) [7, 50, 51] reduced Rab7 Ser72 phosphorylation in wild-type cells (Fig. 2f-g), an effect which was restored following overexpression of LMTK3 (Fig. 2h-i).

To elucidate if Rab7 is directly or indirectly phosphorylated by LMTK3, we performed in vitro kinase assays, using recombinant LMTK3 kinase domain as source of enzyme activity and Rab7 as substrate. Heat shock protein 27 (HSP27) was used as a positive control of LMTK3 phosphorylation [7]. Our results demonstrated that

LMTK3 directly phosphorylates Rab7 in vitro and that this effect is abolished following LMTK3 pharmacological inhibition (Fig. 2j and Figure S2). Moreover, in vitro kinase assays using non-radiolabelled ATP followed by western blotting for Rab7 (phospho-Ser72) further validated the exact phosphorylation residue (Ser72) (Fig. 2k).

To further explore the functional significance of Rab7 phosphorylation at Ser72, single cell clones (T47D and MDA-MB-231) overexpressing wild-type Rab7, Rab7 phospho-mimetic (S72E; Ser72Glu) or phospho-null (S72A; Ser72Ala) mutants were generated (Fig. 2l). Having previously shown that LMTK3 upregulation increases EV size, we explored whether the phospho-mimetic Rab7 mutant (S72E) could recapitulate this effect. NTA of EVs confirmed that S72E mutation significantly increased EV size, mirroring the effects seen on EV biogenesis following LMTK3 overexpression (Fig. 2m). The overexpression of Rab7 mutants did not, however, have any impact on EV number (Fig. 2n). Furthermore, as expected, overexpression of the Rab7 S72A mutant did not alter the EVs, since it did not change the levels of phospho-Rab7 in the cells. Notably, as shown in Fig. 2o-q, the S72E phospho-mimetic Rab7 mutant also leads to enhanced packaging of PSAT1 into EVs, consistent with the effect observed upon overexpression of LMTK3. Together, these data support the hypothesis that LMTK3 alters EV cargo via Rab7 phosphorylation.

#### LMTK3 upregulation disrupts multivesicular body trafficking

To examine the impact of LMTK3 overexpression on a cellular scale, we evaluated whether Rab7 phosphorylation by LMTK3 impacts endosome-lysosome trafficking using an EGFR degradation assay. Rab7 typically interacts with RILP to facilitate the transport of endosomes to lysosomes, however, previous studies have shown that phospho-Rab7 at Ser72 disrupts this interaction [52–54], and as a result, MVBs are degraded at a reduced rate. EGF treatment of serum-starved cells leads to the internalisation of EGFR and its subsequent degradation by the Rab7-dependent transport to the lysosome [54].

Control and LMTK3 overexpressing cells were serum-starved overnight then treated with cycloheximide for one hour. They were then treated with EGF, and western blotting was used to assess EGFR levels at different timepoints. Our results demonstrated that EGFR levels within cells decrease rapidly after EGF treatment in control cells, however the rate of EGFR degradation was reduced in LMTK3 overexpressing cells (Fig. 3a-b), implicating LMTK3 in the fusion process of endosomes with lysosomes and the degradation of endocytic cargo.

Given that Rab7 is integral to the formation of MVBs, and Rab7 deletion has been linked to enlarged MVBs and changes in ILVs [55, 56], we hypothesized that LMTK3-mediated phosphorylation and inactivation of Rab7 would lead to similar changes. TEM analysis of cell sections revealed that LMTK3 overexpression significantly increases both MVB and ILV size (Fig. 3c-e), supporting the hypothesis that LMTK3 alters EV biogenesis through disrupting MVB trafficking, therefore leading to a change in EV subpopulations released by cells. As ILVs are the precursors to exosomes, these data suggest that the regulation of Rab7 by LMTK3 increases EV size through the exosomal pathway.

To further explore if the LMTK3-related changes in MVBs were dependent on Rab7, we used confocal microscopy to examine the impact of LMTK3 overexpression on MVB size in cells with wild-type Rab7 and Rab7 S72A mutant, which cannot be phosphorylated at serine 72. Firstly, Rab7 knockout cells were generated then either Rab7 wild-type or Rab7 S72A were re-expressed in the cells (Fig. 3f). Interestingly, in Rab7 wild-type cells, LMTK3 overexpression caused a significant increase in average MVB size, however this effect did not occur in Rab7 S72A cells, indicating that LMTK3 disrupts MVB dynamics predominantly through phosphorylation of Rab7 at Ser72 (Fig. 3g-h).

In summary, our findings demonstrate that LMTK3 overexpression in breast cancer cells promotes the phosphorylation of Rab7 at Ser72, which in turn disrupts late endosome trafficking and results in the formation of enlarged MVBs. This altered MVB biogenesis drives the production of enlarged EVs with distinct protein cargo, including increased packaging of PSAT1 and LDHB. The data suggest a novel mechanism by which LMTK3 regulates EV biogenesis and trafficking, contributing to its oncogenic potential through the modulation of Rab7 activity.

#### LMTK3 EVs alter the proteome of monocytes and reduce their infiltration into tumour spheroids

The increase in EV size, change in subpopulation distribution, and altered protein cargo unveiled a novel role of LMTK3 in the regulation of EV biogenesis. As EVs influence the behaviour of surrounding cells and considering the contribution of the immune compartment in cancer progression, we next explored the impact of LMTK3 abundance on the BC immune microenvironment.

A computational analysis was conducted to compare LMTK3 expression against the levels of immune cell infiltration, through deconvolution of publicly available BC tumours RNA datasets [34–36]. Our analysis showed significant alterations in different populations of immune cells based on LMTK3 abundance (Fig. 4a and Figure S3). Since monocytes and macrophages were among the significantly altered cell types and acknowledging

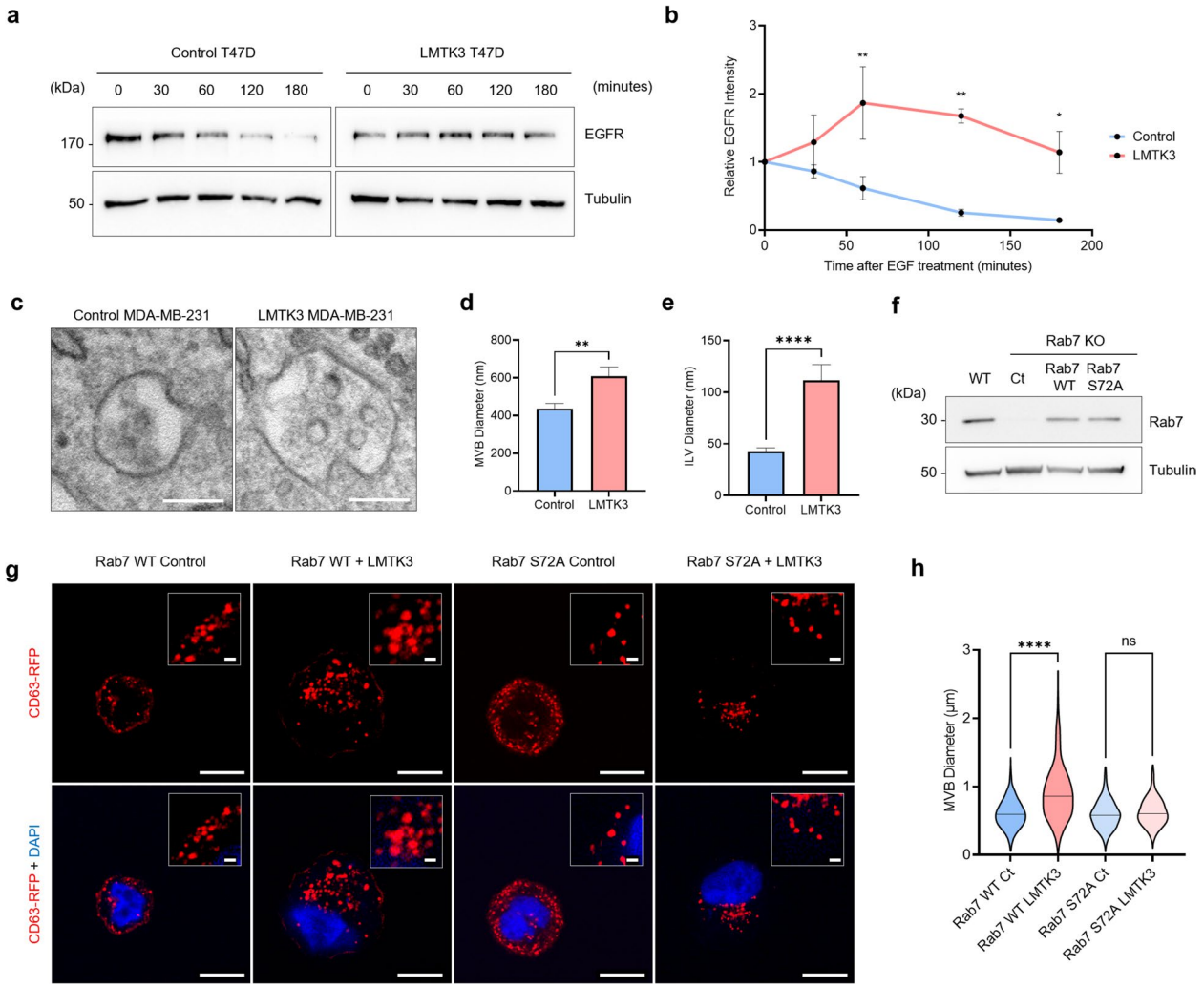


**Fig. 3** Rab7 phosphorylation by LMTK3 increases MVB and ILV size. **a**. Western blot showing EGFR degradation in control and LMTK3 overexpressing T47D. Cells were collected at 0, 30, 60, 120 and 180 min after treatment with EGF. GAPDH is shown as a loading control ($n = 3$). **b**. Quantification of (**a**). *, $p < 0.05$, **, $p < 0.01$ (two-way ANOVA with Bonferroni's multiple comparisons test). **c**. Representative electron micrographs of control and LMTK3 MDA-MB-231. Figure shows MVBs containing ILVs. Images taken at 10,000 × magnification. Scale bars = 200 nm, at least 50 structures were measured per condition from at least 30 fields of view, 3 biological replicates were performed. **d**,**e**. Quantification of (**c**). **f**. Western blot showing Rab7 knockout cells and re-expression of Rab7 wild-type or Rab7 S72 A mutant ($n = 3$). **g**. T47D Rab7 wild-type or Rab7 S72 A cells stably expressing CD63-RFP with and without LMTK3 overexpression were imaged by confocal microscopy to assess changes in MVB diameter. Scale bars = 10 µm or 1 µm (zoom), $n = 500$ MVBs. **h**. Quantification of MVB diameter. Graphs show the mean ± SEM (*$p < 0.05$, **$p < 0.01$, ***$p < 0.001$, ****$p < 0.0001$; one-way ANOVA, followed by Tukey's multiple comparisons test)

that macrophage polarisation is a key factor in the BC TME, we next assessed various M1 (CD80, CD86 and HLA-DRA) and M2 (CD163, TGFB1 and STAT6) macrophage markers in the available clinical samples. Interestingly, M1 markers were reduced in tumours with high levels of LMTK3, while, TGFB1 and STAT6 M2 markers (but not CD163) were upregulated, also highlighting the plasticity and heterogeneity of different subsets of M1/M2-like macrophages [57] (Fig. 4b). Given the key role of monocytes and monocyte-derived cells in BC, and the LMTK3-dependent changes in both monocyte infiltration and macrophage polarisation in clinical samples, we chose to focus exclusively on monocytes in the present study.

Initially, we showed that LMTK3 overexpression in T47D breast cancer cells did not impact the uptake of EVs by monocytes (Figure S4a-S4d). Furthermore, the EVs had no effect on THP-1 proliferation or viability (Figure S4e-S4f). To examine the effect of LMTK3-derived EVs on monocytes in a physiologically relevant setting,

a 3D co-culture assay was used. Briefly, either THP-1 or PBMC-derived monocytes were stained with a green, fluorescent lipophilic tracer and treated with EVs derived from either control or LMTK3-overexpressing T47D cells [58]. High purity monocytes were obtained from PBMCs through plastic adhesion, followed by negative selection using PluriSpin Human Monocyte Enrichment solution (Figure S5a-S5b). A concentration of 10 µg/mL of EV protein was used, which is within the typical range for such functional EV studies [59, 60]. Following EV treatment, monocytes were co-cultured with T47D spheroids to allow infiltration into the tumours (Fig. 4c). Our data demonstrated that LMTK3-derived EVs reduce the infiltration of both immortalised (THP-1) and primary monocytes (PBMC-derived) into BC tumour spheroids (Fig. 4d-g). These results were also validated in MDA-MB-231 spheroids using MDA-MB-231 EVs (Figure S6a-S6b). Additionally, a rescue experiment was carried out where LMTK3 overexpressing cells were treated with C28 and EVs were collected. This abrogated the ability of LMTK3 EVs to reduce monocyte infiltration, suggesting that the effect is specific to LMTK3 (Figure S6c-S6d).

To elucidate the signalling pathways through which the EV-induced changes in monocyte infiltration occur, a proteomics experiment was conducted to assess changes in monocyte protein expression after treatment with LMTK3 EVs. The proteomic analysis identified 15,944 proteins, of which, 1,441 were significantly altered between LMTK3 and control EV-treated monocytes ($p < 0.05$) (Fig. 4h, Figure S6e, Table S2). GO analysis showed enriched proteins are involved in amino acid metabolic processes, catabolic processes and pre-replicative complex assembly (Figure S5c). Among the top upregulated hits were PHGDH, DHX57, CNBP, FAH and REPIN1, and the top downregulated hits included S100A10, KLF13, MTG2, UCHL1, TRPC3 and PIP4P2. Transient receptor potential cation channel subfamily C member 3 (TRPC3) and Ubiquitin C-Terminal Hydrolase L1 (UCHL1) are both known to play roles in promoting M1 macrophage polarisation [61, 62]. Furthermore, S100A10 has been linked to increasing macrophage invasion in tissue [63], therefore downregulation of S100A10 may reduce monocyte infiltration into tumours. In addition, PHGDH upregulation is strongly associated with an M2-like phenotype in macrophages [25].

Monocytes are a source of macrophages in cancer, and macrophages are known to possess several pro- and anti-tumour functions. Given this and the identified differential regulation of proteins involved in macrophage polarisation, we explored the effect of EVs from LMTK3-overexpressing cells on macrophage polarisation. To assess if the EVs were promoting polarisation of the monocytes to either M1 or M2 macrophages, the proteomics data of monocytes treated with EVs was compared with a database of M1 and M2-related protein signatures in macrophages (Fig. 4i) [49]. M1 and M2 polarisation represent the extremes of the macrophage polarisation spectrum, hence macrophages can acquire characteristics of both M1 and M2 macrophages. Nevertheless, this analysis showed that monocytes treated with LMTK3 EVs are more enriched in M2-related proteins than monocytes treated with control EVs. To confirm that this translates into the promotion of M2 polarisation in macrophages, THP-1 monocytes were treated with PMA, triggering macrophage differentiation, then subsequently treated with EVs. RT-qPCR was then used to assess M1 and M2 markers in the treated macrophages (Fig. 4j). LMTK3-derived EVs promoted an M2 phenotype in macrophages with upregulated CD206 and downregulated CD86. Control EVs also led to an increase in

(See figure on next page.)

**Fig. 4** Immune cell infiltration is altered by LMTK3 abundance. **a**. RNA sequencing data and TIMER2.0 infiltration data were used to compare LMTK3 abundance with infiltration of different immune cell populations. Graph shows the mean ± SEM infiltration scores in LMTK3 low vs LMTK3 high samples (*$p < 0.05$, **$p < 0.01$, ***$p < 0.001$, ****$p < 0.0001$; unpaired two-tailed Student's t-test). **b**. Changes in the levels of three M1 and three M2 macrophage markers in breast cancer clinical samples, displayed as mRNA expression z-scores relative to all samples (log RNA Seq V2 RSEM). Q1 (lowest quartile of LMTK3 expression; blue) and Q4 (highest quartile of LMTK3 expression; red) are shown. Graphs show the mean ± SEM (*$p < 0.05$, **$p < 0.01$, ***$p < 0.001$, ****$p < 0.0001$; two-tailed unpaired Student's t-test), $n = 4{,}715$. **c**. Schematic diagram of the spheroid infiltration assay. **d**. Representative images of T47D tumour spheroids with infiltrating monocytes stained in green. **e**. Quantification of (**d**). Data are shown from three biological repeats. Graphs show the mean ± SEM of three independent experiments (*$p < 0.05$, **$p < 0.01$, ***$p < 0.001$, ****$p < 0.0001$; one-way ANOVA, followed by Tukey's multiple comparisons test). **f**,**g**. PBMC-derived monocytes were treated with PBS, control EVs or LMTK3 EVs. They were then co-cultured with T47D tumour spheroids and imaged after 24 h. **f**. Representative images of tumour spheroids with infiltrating monocytes. **g**. Quantification of (**f**). **h**. THP-1 monocytes were treated with either control EVs or LMTK3 EVs. Proteomic analysis revealed changes in the protein expression of the monocytes. Figure shows a volcano plot of the proteomic analysis. X axis shows $\log_2$(fold change) of LMTK3 EV-treated THP-1/Control EV-treated THP-1. Significant upregulated hits are shown in red and downregulated hits in blue. Welch's t test was used to calculate p values. Dotted line indicates $p = 0.05$. **i.** Volcano plot showing proteomics data of control and LMTK3 EV-treated monocytes displaying only proteins involved in M1 or M2 polarisation. Red points are associated with M2 polarisation and blue points are associated with M1 polarisation. **j**. RT-qPCR showing changes in macrophage markers following EV treatment. Graphs show the mean ± SEM of three independent experiments (*$p < 0.05$, **$p < 0.01$, ***$p < 0.001$, ****$p < 0.0001$; one-way ANOVA, followed by Tukey's multiple comparisons test)

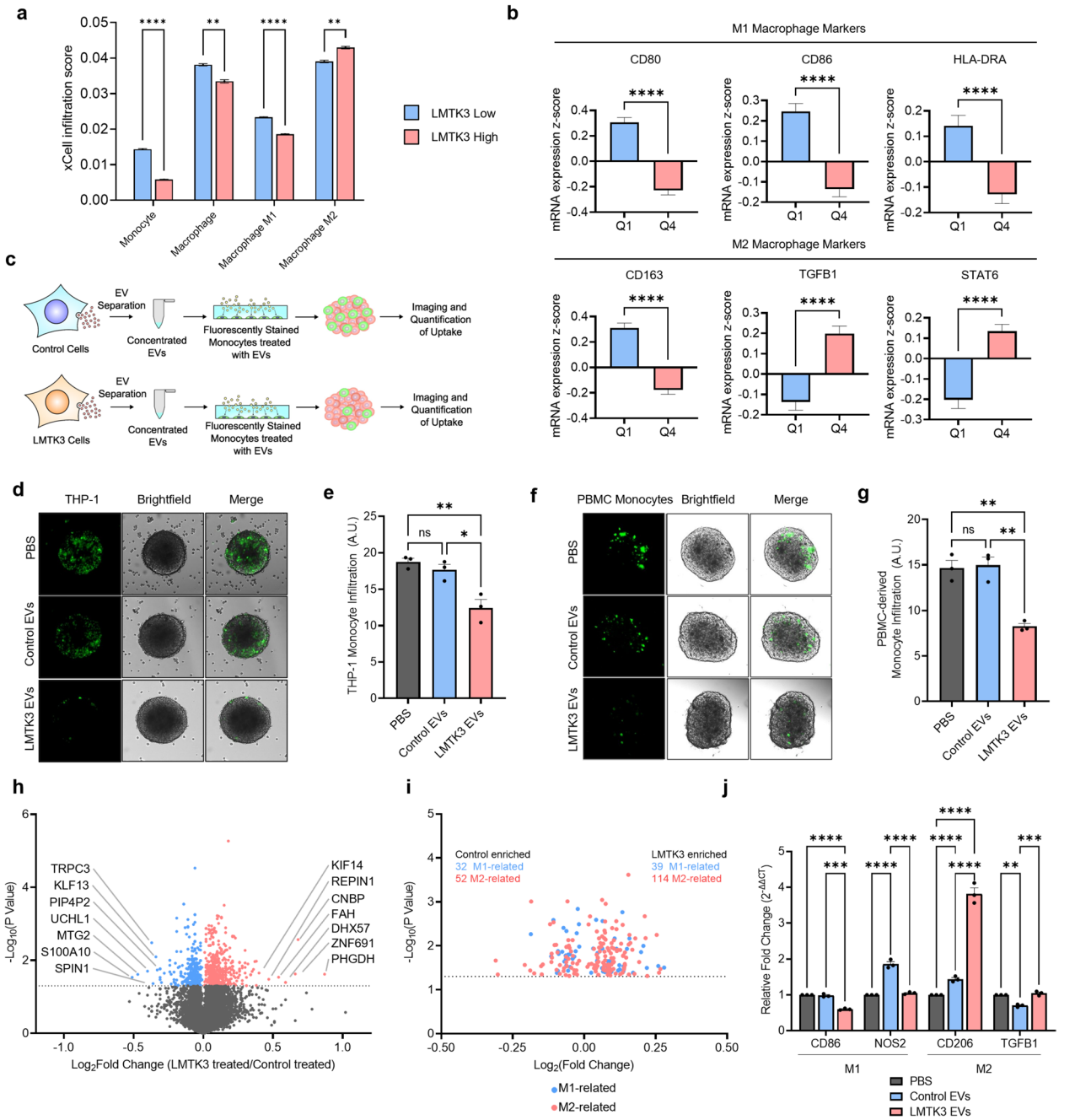


**Fig. 4** (See legend on previous page.)

CD206, however NOS2 was also upregulated and TGFB1 was downregulated. Furthermore, treating LMTK3 overexpressing breast cancer cells with C28 prior to EV collection resulted in a partial abrogation of the M2-promoting ability of the EVs and a full reversal of the inhibition of M1-like gene expression in macrophages (Figure S6f).

Collectively, our data reveal a link between LMTK3 expression and M2 polarisation in macrophages and suggest a possible role for LMTK3 in immunosuppression and evasion of anti-tumour immunity in BC.

### LMTK3 EVs reduce monocyte infiltration in tumour spheroids through PSAT1-PHGDH signalling

Amongst the validated and most upregulated hits upon LMTK3 EV treatment, was phosphoglycerate dehydrogenase (PHGDH), which has been previously described as a metabolic checkpoint of macrophage M2

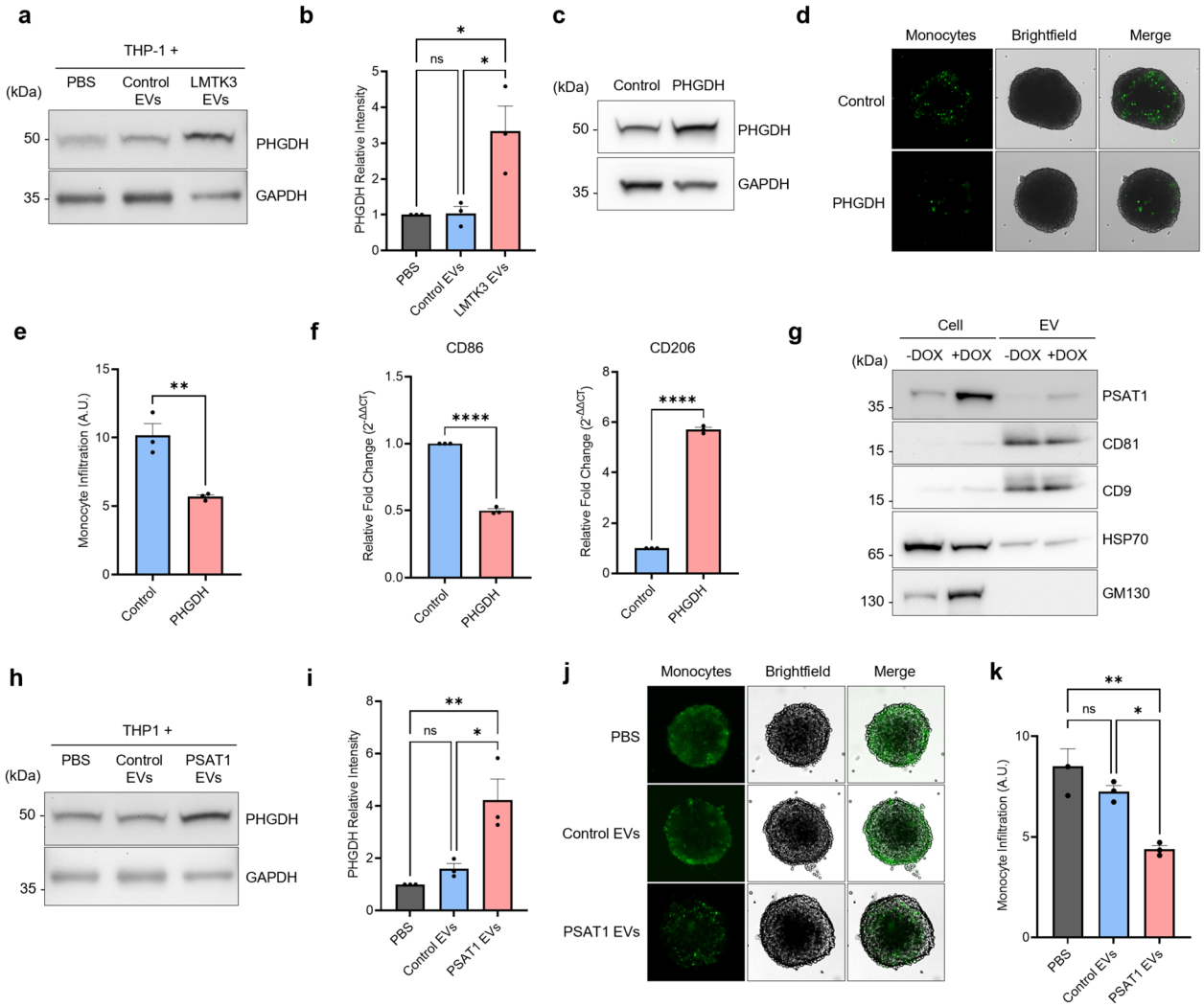


**Fig. 5** LMTK3 EVs promote PSAT1 packaging in EVs, causing an upregulation of PHGDH in monocytes. **a**. Western blot of monocytes treated with PBS, control EVs or LMTK3 EVs. PHGDH was confirmed as upregulated in monocytes treated with LMTK3 EVs. GAPDH is used as a loading control (n = 3). **b**. Quantification of (**a**). **c**. Western blot showing PHGDH overexpression in THP-1 monocytes compared to control monocytes (*n* = 3). **d**. T47D tumour spheroid infiltration assay using control and PHGDH overexpressing monocytes. Monocytes were stained with a green lipophilic tracer. Representative images are shown. **e**. Quantification of (**d**). Graphs show the mean ± SEM of three independent experiments (**p* < 0.05, ***p* < 0.01, ****p* < 0.001, *****p* < 0.0001; as measured by two-tailed unpaired Student's t-test). **f**. RT-qPCR of PHGDH overexpressing monocytes differentiated into macrophages showing upregulation of CD206 and downregulation of CD86 compared to control cells. **g**. A plasmid containing doxycycline-inducible PSAT1 was transfected into MDA-MB-231 and a stable cell line was generated. EVs were collected from the cells with and without doxycycline (24 h). The figure shows a western blot for PSAT1 in the cell lysates and EVs for PSAT1. CD81 and CD9 are used as positive EV markers and an EV loading control. GM130 is used as a negative EV marker and cell lysate loading control (*n* = 3). **h**. THP-1 monocytes were treated with EVs from cells with Dox-inducible PSAT1 overexpression. EVs from MDA-MB-231 cells without doxycycline were used as a control treatment. Vinculin was used as a loading control. Figure is representative of three biological repeats (n = 3). **i.** Quantification of (**h**). **j**. T47D tumour spheroid infiltration assay was carried out using monocytes treated with either PBS, EVs from Dox-inducible PSAT1 MDA-MB-231 without doxycycline or EVs from Dox-inducible PSAT1 MDA-MB-231 with doxycycline. Figure shows representative images from the spheroid infiltration experiment using monocytes treated with EVs from PSAT1 overexpressing cells with and without doxycycline, or PBS. **k**. Quantification of (**i**). Graphs show the mean ± SEM of three independent experiments (**p* < 0.05, ***p* < 0.01, ****p* < 0.001, *****p* < 0.0001; one-way ANOVA, followed by Tukey's multiple comparisons test)

polarisation [25]. PHGDH plays an important role in serine biosynthesis which is a key factor in macrophage polarisation [64]. Other studies have shown that an M2-like phenotype in macrophages is characterised by a reduction in adhesiveness which may explain the reduced rates of infiltration in the spheroid assay [65].

We validated the previous proteomics findings through western blotting to show PHGDH upregulation occurs in THP-1 monocytes following treatment with LMTK3 EVs but not control EVs (Fig. 5a-b). To investigate the potential involvement of PHGDH in monocyte infiltration, we initially established a THP-1 cell line stably overexpressing PHGDH (Fig. 5c) and examined its ability to infiltrate tumour spheroids compared to parental THP-1 cells. Consistent with our hypothesis, PHGDH overexpression caused a significant reduction in monocyte infiltration into breast tumour spheroids (Fig. 5d-e), indicating that the effect of LMTK3-derived EVs on monocyte infiltration can be attributed to PHGDH-mediated signalling. Next, to explore if PHGDH upregulation is sufficient to drive expression of M2-related genes, we performed RT-qPCR analysis on macrophages derived from parental and PHGDH overexpressing monocytes. Interestingly, PHGDH upregulation in monocytes was able to drive CD206 upregulation and reduce CD86 expression consistent with an immunosuppressive phenotype and in agreement with previous studies [28].

Given the downstream serine biosynthesis enzyme PSAT1 was one of the top upregulated proteins in LMTK3 EVs, we hypothesised that transfer of PSAT1 from LMTK3 BC cells to monocytes alters the balance of the intermediary serine biosynthesis metabolites (3-phosphohydroxypyruvate and 3-phosphoserine), triggering upregulation of PHGDH. To test this, PSAT1 was stably overexpressed in BC cells using a doxycycline-inducible overexpression vector, and the cells were expanded for EV collection. The cells were then treated with doxycycline and western blotting was used to confirm overexpression of PSAT1 in the cells and EVs (Fig. 5g). We next explored the ability of PSAT1-overexpressing EVs to promote PHGDH upregulation in monocytes. Conditioned media was collected from the PSAT1 overexpressing BC cells with and without the addition of doxycycline, and the EVs were separated and used to treat THP-1 monocytes. Western blotting analysis confirmed that PSAT1 abundance in EVs can significantly increase PHGDH protein levels in monocytes (Fig. 5h-i). Moreover, we assessed the potential of EVs with upregulated PSAT1 to decrease tumour spheroid infiltration. As anticipated, the spheroid infiltration assay showed that BC EVs with upregulated PSAT1 levels can reduce monocyte infiltration in spheroids (Fig. 5j-k), to a comparable degree to that induced via treatment with LMTK3-derived EVs, resulting in a similar phenotype.

Overall, these data show that BC cells-derived EVs containing PSAT1 are sufficient to induce paracrine upregulation of PHGDH in monocytes, which ultimately leads to reduced infiltration of monocytes in tumour spheroids.

#### LMTK3 promotes an immunosuppressive phenotype in macrophages in vivo

Following the in vitro studies demonstrating that LMTK3-dependent EV cargo promotes M2-like polarisation in macrophages and exclusion of monocytes in breast tumour spheroids, we sought to investigate the effects of LMTK3 overexpression in an in vivo syngeneic model, using the immunodeficient mouse strain *Rag1*$^{-/-}$ C57Bl/6. These mice are unable to produce mature adaptive immune cells, including T cells due to impaired V(D)J recombination, inhibiting T and B cell development, however, innate immune cells are unaffected and develop normally, preserving monocyte and macrophage function. We initially established a mouse mammary carcinoma cell line (MMTV-Neu) stably overexpressing LMTK3 (Fig. 6a-b) and next, EVs were collected from these cells and compared to the control cells to assess LMTK3-dependent changes in EV protein cargo. Based on our aforementioned results and proposed mechanism, we examined the expression of PSAT1 in MMTV-Neu cells and confirmed its elevated packaging into EVs following LMTK3 upregulation (Fig. 6c).

Parental and LMTK3-overexpressing MMTV-Neu cells were then injected into *Rag1*$^{-/-}$ C57Bl/6 mice and allowed to form tumours in both flanks of the mice and the tumours were measured twice per week. Consistent with previous studies [1, 5, 7, 8], overexpression of LMTK3 in the MMTV-Neu cells resulted larger tumours (Fig. 6d-e). Furthermore, the LMTK3 tumours displayed higher levels of ki-67 compared to control tumours, providing additional evidence that LMTK3 promotes proliferation of BC cells (Fig. 6f-g).

Following dissociation of the tumours, we assessed the infiltration of innate immune cells (monocytes and monocyte-derived macrophages) into the tumours via flow cytometry analysis of CD45, CD11b and F4/80 positive cells (monocytes/macrophages). Our data showed that LMTK3 overexpressing tumours have a reduced level of monocyte infiltration in vivo, in agreement with the clinical analysis of human cancers and our in vitro data demonstrating that LMTK3 EVs exclude monocytes from tumour spheroids (Fig. 6h). In addition, these tumours had increased levels of M2-like macrophages and decreased levels of M1-like macrophages compared to control tumours (Fig. 6i-k). These data further validate the tumour promoting role of macrophage PHGDH, as previously described [25, 28] and a novel tumour promoting role of LMTK3 by manipulating the TME and favouring immunosuppression through EV-dependent upregulation of PHGDH in monocytes. These results

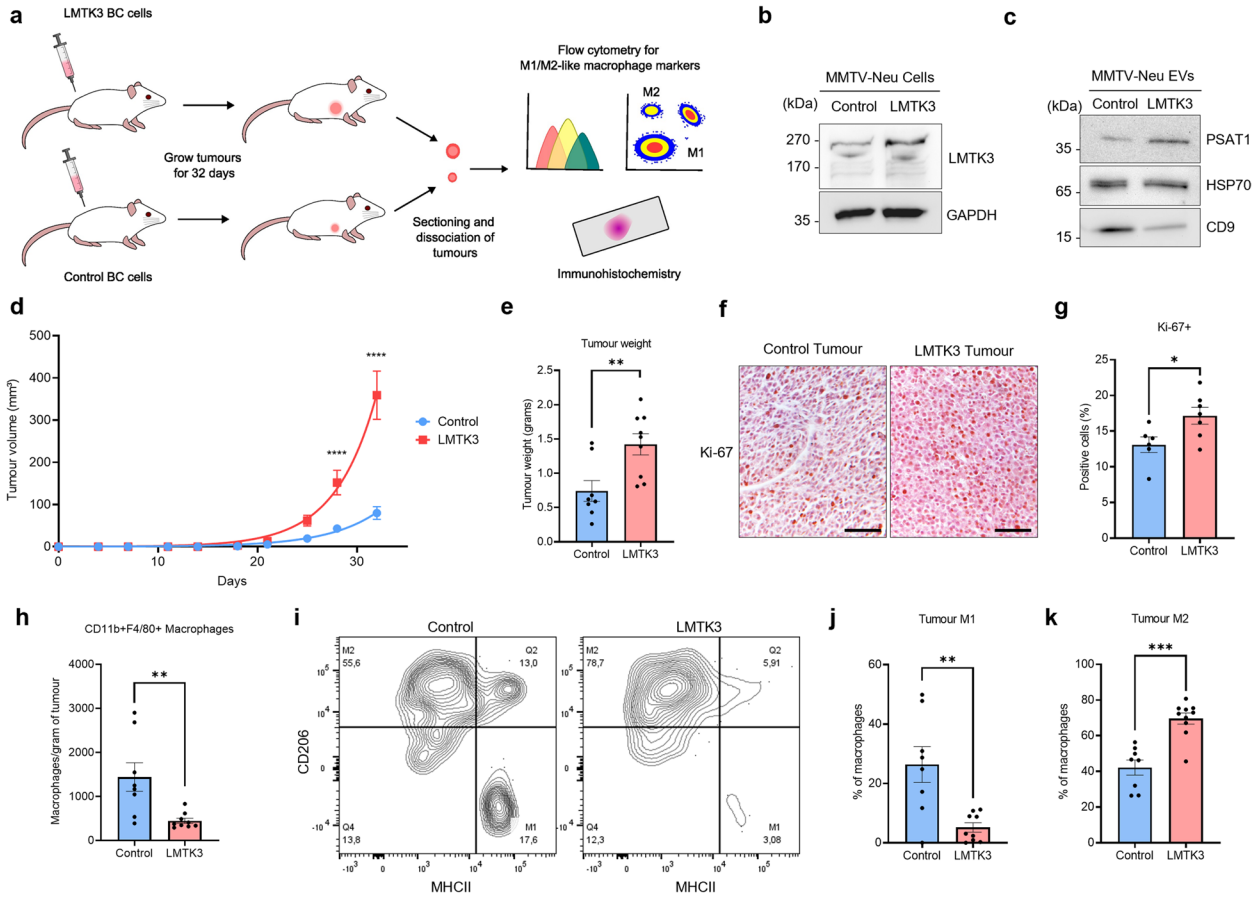


**Fig. 6** LMTK3 alters monocyte behaviour and macrophage polarisation in vivo. **a**. Schematic diagram showing the experimental procedure where mice were injected with breast cancer cells that were allowed to form tumours. Tumours were then measured and analysed by flow cytometry and IHC. **b**. Western blot showing LMTK3 overexpression in MMTV-Neu mouse mammary carcinoma cells. GAPDH is shown as a loading control (n = 3). **c.** Western blot showing overexpression of LMTK3 in MMTV-Neu cells results in upregulation of PSAT1 in EVs. HSP70 was used as a loading control ($n$ = 3). **d**. Tumours were measured twice per week with callipers. Tumour volume is displayed in $mm^3$ (two-way ANOVA with Bonferroni's multiple comparisons test). **e**. Tumour weights on day 32. Graphs show the mean ± SEM *$p < 0.05$, **$p < 0.01$, ***$p < 0.001$; two-tailed unpaired Student's t-test. n = 8 tumours (control) and n = 9 tumours (LMTK3). **f**. IHC analysis of ki-67 positive nuclei. Representative images are shown. Scale bar = 100 µm. **g**. Quantification of (**f**). Graph shows the mean ± SEM as measured by two-tailed unpaired Student's t-test. **h**. Tumours were dissociated and stained for CD45, CD11b and F4/80. Triple-positive cells were counted and normalised to tumour weights. Graph shows number of macrophages per gram of tumour. Graph shows the mean ± SEM; two-tailed unpaired Student's t-test. n = 8 control and 9 LMTK3 tumours. **i.** Representative flow cytometry of cells indicating M1 and M2-like macrophages in dissociated tumours. **j**,**k**. Flow cytometry showing percentage of M1- (**j**) and M2-like (**k**) macrophages in tumours. Graphs show the mean ± SEM *p < 0.05, **p < 0.01, ***p < 0.001; two-tailed unpaired Student's t-test

were also replicated in a separate syngeneic female mouse cohort using orthotopic injection of tumour cells, confirming the observed immunosuppressive and growth promoting effects of LMTK3 overexpression (Figure S7).

### LMTK3 EVs directly contribute to immunosuppressive macrophage phenotype in vivo

To assess the contribution of LMTK3 EVs specifically to tumour growth and macrophage polarisation, we conducted an in vivo model where 4T1 cells were used to form tumours in BALB/c mice (Fig. 7a). The mice were subsequently treated with intratumoural injections of T47D- or MDA-MB-231-derived EVs from either control or LMTK3 overexpressing cells. Tumours were measured three times per week and were used for flow cytometry to assess infiltrating macrophage polarisation.

Our results showed that LMTK3 EVs from both cell lines (T47D and MDA-MB-231) increase tumour growth (Fig. 7b-i), albeit to a lesser extent, as expected, than LMTK3 overexpression does in our previous model (Fig. 6d). This is consistent with the various

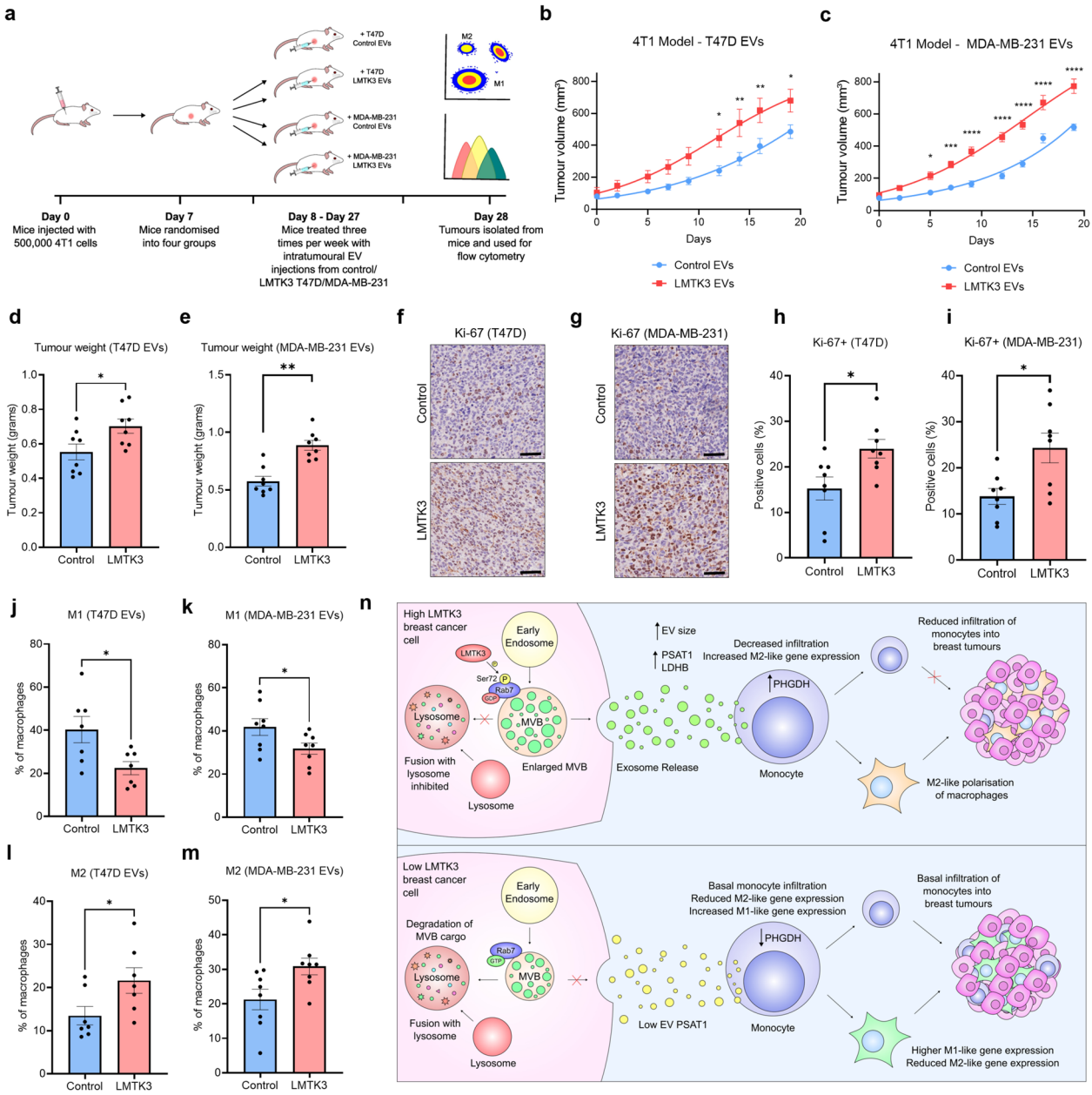


**Fig. 7** LMTK3 EVs increase tumour growth and promote an immunosuppressive phenotype in infiltrating macrophages. **a**. Schematic diagram showing mice were injected with 4T1 cells to form tumours. Mice were then randomised and treated with 50 µg of EVs three times per week. Tumours were analysed with flow cytometry. **b**,**c**. Tumour growth curves showing tumour volume in $mm^3$ for mice treated with T47D EVs (**b**) and MDA-MB-231 EVs (**c**) (two-way ANOVA with Bonferroni's multiple comparisons test). **d,e**. Graphs show the final tumour weights (grams) for 4T1 mouse models treated with T47D (**d**) or MDA-MB-231 (**e**) EVs. Graphs show mean ± SEM *$p < 0.05$, **$p < 0.01$; two-tailed unpaired Student's t-test. n = 8 tumours per condition. **f**,**g**. IHC analysis of 4T1 tumours for ki-67 positive nuclei. Representative images are shown. Scale bar = 50 µm**.** **h**,**i**. Quantification of (**f**,**g**). Graph shows the mean ± SEM, *$p < 0.05$ as measured by two-tailed unpaired Student's t-test. **j-m**. Flow cytometry showing percentage of M1- (**j**,**k**) and M2-like (**l**,**m**) macrophages in tumours. Graphs show the mean ± SEM *p < 0.05; two-tailed unpaired Student's t-test. **n**. Proposed model showing LMTK3 overexpression in breast cancer cells results in increased serine 72 phosphorylation of Rab7. This alters MVB trafficking, resulting in increased packaging of PSAT1 into EVs. These EVs are taken up by monocytes, causing an upregulation of PHGDH, resulting in an M2-like phenotype in monocyte-derived macrophages and reduced infiltration

additional oncogenic roles of LMTK3 apart from regulating EV biogenesis. Furthermore, LMTK3 EVs were sufficient to decrease M1-like gene expression (MHC-II) and increase M2-like gene expression (CD206) in tumour-infiltrating macrophages (Fig. 7j-m).

Taken together, these data show a direct link between LMTK3-dependent EVs and tumour growth and demonstrate that LMTK3 EVs promote an immunosuppressive M2-like phenotype in macrophages (Fig. 7n).

## Discussion

In recent years, EVs have gained considerable interest for their role in cellular communication, particularly in cancer [41, 66]. EV-mediated transport of proteins, lipids, and nucleic acids enables cancer cells to influence numerous physiological processes in a variety of cell types across distances. Given the strong involvement of EVs in cancer biology, understanding the mechanisms governing their biogenesis, cargo selection, release and uptake has become an important goal in cancer research. Despite numerous advances in knowledge of how EV biogenesis occurs, many questions remain, particularly regarding selective loading mechanisms of EVs and how these processes could be manipulated for therapeutic purposes. As EVs are increasingly recognised as key regulators of oncogenic features in the TME, investigating regulatory mechanisms governing their biogenesis and specific pathways influencing their size, cargo and subpopulations is critical.

Among the many impacts of EVs, one of the most significant may be their ability to facilitate tumour progression through manipulation of the TME. A wealth of research has shown that EVs play a central role in TME modulation through the transfer of bioactive cargo. EVs have been implicated in several different oncogenic processes within the TME, including cancer-associated fibroblast induction, changes in vasculature, and metastasis. Furthermore, EVs have several immune-regulating functions where they suppress anti-cancer immunity, promote immune tolerance and support cancer escape from immune surveillance. Recent studies have shown that EVs can impact the composition of tumours, recruiting pro-tumourigenic cells and excluding or suppressing cytotoxic anti-tumour cells [66]. In addition, several studies have also explored the link between EVs and macrophage polarisation in cancer [67]. Given the recent advancements in immunotherapies, including checkpoint inhibitors and CAR T-cell therapies, it is increasingly important to further understand the factors governing immune regulation in cancer.

LMTK3 is a well-established oncogenic protein kinase with known roles in promoting BC growth, metastasis and therapy resistance [3–5, 7, 8]. However, its involvement in EV biogenesis and its contribution in the TME have not previously been explored. Preliminary evidence suggests LMTK3 may have a role in endosomal trafficking, however, this is limited to studies in normal physiology with much less evidence shedding light on its roles in trafficking and immune regulation in cancer [8]. Considering that previous studies have mainly linked the upregulation of LMTK3 protein levels with cancer development (instead of LMTK3 mutations, which are in general very rare in different malignancies) [3–5, 7, 8], we explored the impact of LMTK3 upregulation in this study in order to assess its role in EV biogenesis.

The current study is the first to demonstrate that LMTK3 upregulation in cells impacts EV size, protein cargo and subpopulation distribution, revealing a novel mechanism whereby LMTK3 modulates EV biogenesis through Rab7 regulation. Furthermore, we present evidence that links LMTK3 expression with an immunosuppressive TME. Overexpression of LMTK3 in a panel of BC cell lines led to a significant increase in the average size and subpopulation distribution of EVs, highlighting its role in a fundamental aspect of EV biogenesis. As EV size is linked to properties such as release, internalisation, diffusion and clearance, this alteration may have functional consequences in cancer. For instance, these larger EVs may exhibit different rates of internalisation or biodistribution as EV size is known to alter these properties; however, this requires further exploration [68, 69]. Moreover, LMTK3-altered proteomic cargo of EVs, including proteins involved in amino acid transport, can influence the intercellular communications within the TME. Interestingly, the identification of LMTK3 as a cargo protein inside the EVs suggests another mechanism by which LMTK3 may propagate its oncogenic effects to nearby cells. Additionally, LMTK3-mediated downregulation of CD63-positive EV particles, which are traditionally associated with EVs generated through the tetraspanin-dependent exosome biogenesis pathway [70], suggests that LMTK3 mainly influences the biogenesis of exosomes rather than other subtypes of EVs.

The subcellular localisation of LMTK3 to the late endosomal membrane further suggests that this altered biogenesis involves the exosomal pathway of EV biogenesis. Rab7 is known to regulate MVB trafficking and phosphorylation of Rab7 at Ser72 is linked to changes in GTPase activity and decreased association with the Rab7 effector, RILP [71]. Rab7 has a complex role in vesicle trafficking. One study showed that Rab7 positively regulates EV secretion [72], whereas others have shown the opposite effect [71]. Here, we identified Rab7 as a novel phosphorylation substrate of LMTK3 and, via gain- and loss- of function experiments we demonstrated that LMTK3-mediated phosphorylation of Rab7

at Ser72 is sufficient to cause the increase in EV size and altered protein cargo. In addition to mediating intercellular communication, EVs are thought to be an energetically favourable mechanism allowing cells to expel waste, particularly for proteins that are hard to degrade. This regulation of Rab7 may therefore represent a switch from lysosomal degradation to expulsion of waste through EVs, however, further investigation is needed into this.

Our findings have important implications for understanding BC progression and EV-mediated intercellular communication. The ability of LMTK3 to alter EV size, cargo, and subpopulation distribution suggests a critical role in modifying the TME and promoting tumour progression. As EVs are known to alter many processes, including angiogenesis, invasion and immune evasion, LMTK3 may enhance these pro-tumourigenic interactions, promoting the progression of BC through a novel process. Targeting LMTK3 or its downstream effector Rab7 may therefore reduce the oncogenic potential of BC EVs, impairing the ability of the TME to promote growth. Therefore, the subsequent exploration of the role of LMTK3-dependent EVs on the TME was essential.

Deconvolution of RNA sequencing data from BC patients identified monocytes being downregulated in LMTK3 overexpressed BCs. It is unclear why monocytes are excluded from the tumours, however, in early BC, the microenvironment is pro-inflammatory, and cancers must evade immune detection to survive [72, 73]. The exclusion of monocytes may represent a strategy where the cancer cells delay the infiltration of myeloid cells until a pro-tumourigenic microenvironment is well-established. Still, this is yet to be determined and analysis of clinical data from BC patients at different stages would provide further information on this matter. Additionally, M2 macrophage markers were increased and M1 macrophage markers were decreased in LMTK3 upregulated BC patients. In accordance with the many tumour-promoting roles of LMTK3, the polarisation of macrophages to an M2-like phenotype may also contribute to the poorer survival in patients with higher levels of LMTK3. In addition to monocytes, other immune cell populations were also affected. Interestingly, some populations of T cells were downregulated in tumours expressing high LMTK3 levels, as it is expected in response to an increase of immunosuppressive macrophages. This finding further supports the hypothesis that LMTK3 upregulation contributes to an immunosuppressive microenvironment.

Our in vitro work showed that LMTK3 EVs are not taken up at a different rate compared to control EVs and they do not impact THP-1 monocytes proliferation or viability. This shows that the effects observed are specific to changes in monocyte function, rather than altered uptake, cytotoxicity or effects on proliferation. LMTK3 EVs reduced monocyte infiltration into tumour spheroids, mirroring the clinical data and suggesting that LMTK3-regulated EVs are responsible to an extent for this effect, instead of cytokines or other cell–cell signalling mechanisms. To further explore this in our models, we analysed the proteomic content of monocytes and revealed that LMTK3 EVs can differentially affect monocyte protein expression. Notably, PHGDH, a key protein involved in serine biosynthesis and macrophage M2 polarisation [25, 28], was amongst the main hits upregulated in monocytes treated with LMTK3 EVs. We showed that PHGDH overexpression is sufficient for reducing their infiltration into tumour spheroids, showing that the effects of LMTK3-derived EVs can be attributable PHGDH signalling. Furthermore, we provide evidence that LMTK3 EVs drive M2 polarisation in monocyte-derived macrophages. M2 macrophages perform a wide range of pro-tumourigenic functions, promoting tumour growth, metastasis and drug resistance [57]. We have also shown that LMTK3 overexpression in breast cancer causes the release of EVs that promote M2 polarisation in macrophages lending further evidence to the tumour-promoting role for LMTK3 in breast cancer.

The ability of LMTK3 EVs to increase the rate of tumour growth and promote M2-like macrophage polarisation suggests that LMTK3-dependent changes in EV protein cargo contribute, at least partly, to these pro-tumourigenic effects. As anticipated, the magnitude of the effects was stronger in the mouse model comparing control and LMTK3 overexpressing cells than in the EV mouse model. This difference may be attributable to several factors, including differences in the cancer cell lines used, differences in the mice or the dose of EVs, as continuous EV secretion by tumour cells cannot be perfectly replicated by intermittent intratumoural injections. Nevertheless, both models clearly demonstrate that LMTK3-modulated EVs have both pro-tumourigenic and immunomodulatory properties.

Examining the upstream regulation of PHGDH upregulation in monocytes revealed that PSAT1 is an important EV cargo protein that promotes PHGDH upregulation in monocytes and subsequent decrease in monocytes infiltration into tumours. This effect could be mediated via increased flux through the serine biosynthesis pathway, thereby increasing metabolic states in the cells. As PSAT1 and PHGDH are often co-upregulated in cells during surges in metabolic demand, it is possible that the increase in EV PSAT1 and transfer to monocytes is sufficient to induce PHGDH upregulation, triggering the observed changes in the phenotype. In addition to PHGDH upregulation, S100A10 was also downregulated in monocytes treated with LMTK3 EVs. S100A10

is a known regulator of macrophage invasion, therefore it may also play a role in the process [63]. Whilst clarifying the exact mechanism of action was beyond the scope of the present study, future work could ultimately serve to elucidate this further. Previous studies have also implicated other hits in macrophage polarisation, including TRPC3 and UCHL1, which were among the top hits altered in monocytes treated with LMTK3 EVs, therefore, additional changes may also contribute to the M2 phenotype observed [61, 62].

The in vivo mouse models also supported the in vitro data, demonstrating that LMTK3 upregulation in BC is tumourigenic. Furthermore, the flow cytometry results showed that M2-like macrophages are upregulated, and M1-like macrophages are downregulated in LMTK3 overexpressing tumours. Future work using cell type-specific deletions of PSAT1 and PHGDH would be useful to provide further evidence to this mechanism.

Overall, our experiments support that LMTK3 EVs are pro-tumourigenic in the BC immune TME. The alterations in EV protein cargo appear to be crucial in modulating the immune TME through regulation of monocytes and macrophage polarisation, promoting a pro-tumourigenic environment. Further research into their action on other cell types in the TME will be crucial to gaining a full understanding of the LMTK3-dependent changes in the TME and how this could be used to inform clinical decisions.

#### Abbreviations

| | |
|---|---|
| ANOVA | Analysis Of Variance |
| BC | Breast Cancer |
| CD | Cluster Of Differentiation |
| CRC | Colorectal Cancer |
| DAPI | 4',6-Diamidino-2-Phenylindole |
| DMEM | Dulbecco's Modified Eagle Medium |
| DUC | Differential Ultracentrifugation |
| ERa | Estrogen Receptor A |
| EV | Extracellular Vesicle |
| FBS | Foetal Bovine Serum |
| GO | Gene Ontology |
| HRP | Horseradish Peroxidase |
| HSP27 | Heat Shock Protein 27 |
| ILV | Intraluminal Vesicle |
| LDHB | Lactate Dehydrogenase B |
| LMTK3 | Lemur Tail Kinase 3 |
| MVB | Multivesicular Body |
| NK | Natural Killer |
| NMDA | N-Methyl D-Aspartate |
| NTA | Nanoparticle Tracking Analysis |
| P/S | Penicillin/Streptomycin |
| PBMC | Peripheral Blood Mononuclear Cells |
| PBS | Phosphate Buffered Saline |
| PHGDH | Phosphoglycerate Dehydrogenase |
| PMA | 12-0-Tetradecanoylphorbol-13-Acetate |
| PSAT1 | Phosphoserine Aminotransferase 1 |
| RILP | Rab-Interacting Lysosomal Protein |
| RIPA | Radioimmunoprecipitation Assay |
| ROS | Reactive Oxygen Species |
| RPMI-1640 | Roswell Park Memorial Institute 1640 |
| SEM | Standard Error of The Mean |
| SP-IRIS | Single Particle Interferometric Reflectance Imaging Sensor |
| TAM | Tumour-Associated Macrophages |
| TCGA | The Cancer Genome Atlas |
| TEM | Transmission Electron Microscopy |
| Th1 | T Helper 1 |
| TIMER | Tumour Immune Estimation Resource |
| TME | Tumour Microenvironment |
| TMT | Tandem Mass Tag |
| TNF-α | Tumour Necrosis Factor Alpha |
| TRPC3 | Transient Receptor Potential Cation Channel Subfamily C Member 3 |
| UCHL1 | Ubiquitin C-Terminal Hydrolase L1 |

## Supplementary Information

The online version contains supplementary material available at https://doi.org/10.1186/s12943-025-02346-2.

Supplementary Material 1.

#### Acknowledgements

We would like to thank Dr Pascale Schellenberger for her technical support in performing the electron microscopy analysis of EVs. We also want to thank Dr Zhu Feiye, Tai Yan and Wang Bo for assisting with the sample preparation and imaging of MVBs. In addition, we would like to thank Dr Katiuscia Bianchi for providing the PHGDH and PSAT1 overexpression plasmids. We would also like to thank Dr Meiya Li for assisting with the flow cytometry of dissociated 4T1 tumours (Fig. 7). We also want to thank Fangming Chen, Xiaoqin Jin and Shujun Dong for performing the IHC staining of the 4T1 tumours (Figure 7).

#### Authors' contributions

Methodology: M.S., C.K., S.B., A.L.B., K.T., C.T., R.S.N., N.P., W.J., K.T.; formal analysis: M.S., C.K., K.T., A.K.; investigation: M.S., S.B., A.L.B., C.K., K.T., W.J., R.S.N., N.P., C.T., R.G.; writing—original draft preparation: M.S., S.B., W.J., G.G.; writing—review and editing: M.S., C.K., W.J., A.L.B., S.B., C.T., A.K., G.G.: supervision, G.G: funding acquisition, G.G. All authors have read and agreed to the published version of the manuscript.

#### Funding

This research was funded by a funded PhD studentship (Mark Samuels) from the School of Life Sciences at the University of Sussex and by Action Against Cancer, grant number ID6292/G1828 awarded to Professor Georgios Giamas.

#### Data availability

The datasets supporting the conclusions of this article are included within the article and its additional files. The proteomics datasets are available as supplementary tables 1 and 2.

## Declarations

#### Ethics approval and consent to participate

The research in this study using PBMCs was approved by the research ethics committee of Sciences and Technology (C-REC) at the University of Sussex (Reference Number: ER/MS2207/1) on the 14 th of June 2023. Written informed consent was obtained from all study participants.
The animal studies were conducted in in the Animal House Facility of the Biomedical Research Foundation of the Academy of Athens (BRFAA, Greece). All procedures for the care and treatment of the animals were approved by the Institutional Committee on Ethics of Animal Experiments, and studies were conducted in full compliance with FELASA (Federation of Laboratory Animal Science Associations) recommendations. Ethics number: 1385947/27–12-2022.
The 4T1 mouse model was conducted in the animal experiment centre of Zhejiang Chinese Medicine University. Mouse experiments were approved by the Experimental Animal Ethics Committee of Zhejiang Chinese Medicine University (approval number: IACUC-20250120–18).

#### Consent for publication

Not applicable.

**Competing interests**
The authors declare no competing interests.

**Author details**
[1]International Oncology Institute, The First Affiliated Hospital of Zhejiang Chinese Medical University. Oncology department of the first affiliated Hospital of Zhejiang Chinese Medical University, Hangzhou 310053, China. [2]Department of Biochemistry and Biomedicine, School of Life Sciences, University of Sussex, JMS Building, Falmer, Brighton BN1 9QG, UK. [3]Center of Basic Research Biomedical Research Foundation of the Academy of Athens, Athens 11527, Greece. [4]Sussex Neuroscience, School of Life Sciences, University of Sussex, Brighton, UK.

Received: 9 January 2025 Accepted: 28 April 2025
Published online: 23 May 2025

**References**

1. Xu Y, Zhang H, Lit LC, Grothey A, Athanasiadou M, Kiritsi M, et al. The kinase LMTK3 promotes invasion in breast cancer through GRB2-mediated induction of integrin beta(1). Sci Signal. 2014;7(330):ra58.
2. Stebbing J, Filipovic A, Lit LC, Blighe K, Grothey A, Xu Y, et al. LMTK3 is implicated in endocrine resistance via multiple signaling pathways. Oncogene. 2013;32(28):3371–80.
3. Xu Y, Zhang H, Nguyen VT, Angelopoulos N, Nunes J, Reid A, et al. LMTK3 Represses Tumor Suppressor-like Genes through Chromatin Remodeling in Breast Cancer. Cell Rep. 2015;12(5):837–49.
4. Stebbing J, Shah K, Lit LC, Gagliano T, Ditsiou A, Wang T, et al. LMTK3 confers chemo-resistance in breast cancer. Oncogene. 2018;37(23):3113–30.
5. Giamas G, Filipovic A, Jacob J, Messier W, Zhang H, Yang D, et al. Kinome screening for regulators of the estrogen receptor identifies LMTK3 as a new therapeutic target in breast cancer. Nat Med. 2011;17(6):715–9.
6. Jacob J, Favicchio R, Karimian N, Mehrabi M, Harding V, Castellano L, et al. LMTK3 escapes tumour suppressor miRNAs via sequestration of DDX5. Cancer Lett. 2016;372(1):137–46.
7. Ditsiou A, Cilibrasi C, Simigdala N, Papakyriakou A, Milton-Harris L, Vella V, et al. The structure-function relationship of oncogenic LMTK3. Sci Adv. 2020;6(46).
8. Ditsiou A, Gagliano T, Samuels M, Vella V, Tolias C, Giamas G. The multifaceted role of lemur tyrosine kinase 3 in health and disease. Open Biol. 2021;11(9): 210218.
9. Wendler F, Purice TM, Simon T, Stebbing J, Giamas G. The LMTK-family of kinases: Emerging important players in cell physiology and pathogenesis. Biochim Biophys Acta Mol Basis Dis. 2021;1867(9): 165372.
10. Chibalina MV, Seaman MN, Miller CC, Kendrick-Jones J, Buss F. Myosin VI and its interacting protein LMTK2 regulate tubule formation and transport to the endocytic recycling compartment. J Cell Sci. 2007;120(Pt 24):4278–88.
11. Homma Y, Hiragi S, Fukuda M. Rab family of small GTPases: an updated view on their regulation and functions. FEBS J. 2021;288(1):36–55.
12. Bucci C, Thomsen P, Nicoziani P, McCarthy J, van Deurs B. Rab7: a key to lysosome biogenesis. Mol Biol Cell. 2000;11(2):467–80.
13. Luzio JP, Pryor PR, Bright NA. Lysosomes: fusion and function. Nat Rev Mol Cell Biol. 2007;8(8):622–32.
14. Gurung S, Perocheau D, Touramanidou L, Baruteau J. The exosome journey: from biogenesis to uptake and intracellular signalling. Cell Commun Signal. 2021;19(1):47.
15. Wendler F, Stamp GW, Giamas G. Tumor-Stromal Cell Communication: Small Vesicles Signal Big Changes. Trends Cancer. 2016;2(7):326-9.
16. Kapellos TS, Bonaguro L, Gemund I, Reusch N, Saglam A, Hinkley ER, Schultze JL. Human Monocyte Subsets and Phenotypes in Major Chronic Inflammatory Diseases. Front Immunol. 2019;10:2035.
17. Gren ST, Rasmussen TB, Janciauskiene S, Hakansson K, Gerwien JG, Grip O. A Single-Cell Gene-Expression Profile Reveals Inter-Cellular Heterogeneity within Human Monocyte Subsets. PLoS ONE. 2015;10(12): e0144351.
18. Feng AL, Zhu JK, Sun JT, Yang MX, Neckenig MR, Wang XW, et al. CD16+ monocytes in breast cancer patients: expanded by monocyte chemoattractant protein-1 and may be useful for early diagnosis. Clin Exp Immunol. 2011;164(1):57–65.
19. Wang YH, Shen CY, Lin SC, Kuo WH, Kuo YT, Hsu YL, et al. Monocytes secrete CXCL7 to promote breast cancer progression. Cell Death Dis. 2021;12(12):1090.
20. Azizi E, Carr AJ, Plitas G, Cornish AE, Konopacki C, Prabhakaran S, et al. Single-Cell Map of Diverse Immune Phenotypes in the Breast Tumor Microenvironment. Cell. 2018;174(5):1293–308 e36.
21. Bronte V. Deciphering Macrophage and Monocyte Code to Stratify Human Breast Cancer Patients. Cancer Cell. 2019;35(4):538–9.
22. Chen S, Saeed A, Liu Q, Jiang Q, Xu H, Xiao GG, et al. Macrophages in immunoregulation and therapeutics. Signal Transduct Target Ther. 2023;8(1):207.
23. Amer HT, Stein U, El Tayebi HM. The Monocyte, a Maestro in the Tumor Microenvironment (TME) of Breast Cancer. Cancers (Basel). 2022;14(21).
24. Toor SM, Syed Khaja AS, El Salhat H, Faour I, Kanbar J, Quadri AA, et al. Myeloid cells in circulation and tumor microenvironment of breast cancer patients. Cancer Immunol Immunother. 2017;66(6):753–64.
25. Wilson JL, Nagele T, Linke M, Demel F, Fritsch SD, Mayr HK, et al. Inverse Data-Driven Modeling and Multiomics Analysis Reveals Phgdh as a Metabolic Checkpoint of Macrophage Polarization and Proliferation. Cell Rep. 2020;30(5):1542–52 e7.
26. Shan X, Hu P, Ni L, Shen L, Zhang Y, Ji Z, et al. Serine metabolism orchestrates macrophage polarization by regulating the IGF1-p38 axis. Cell Mol Immunol. 2022;19(11):1263–78.
27. Wang C, Chen Q, Chen S, Fan L, Gan Z, Zhao M, et al. Serine synthesis sustains macrophage IL-1beta production via NAD(+)-dependent protein acetylation. Mol Cell. 2024;84(4):744–59 e6.
28. Cai Z, Li W, Hager S, Wilson JL, Afjehi-Sadat L, Heiss EH, et al. Targeting PHGDH reverses the immunosuppressive phenotype of tumor-associated macrophages through alpha-ketoglutarate and mTORC1 signaling. Cell Mol Immunol. 2024;21(5):448–65.
29. Du M, Gu D, Xin J, Peters U, Song M, Cai G, et al. Integrated multi-omics approach to distinct molecular characterization and classification of early-onset colorectal cancer. Cell Rep Med. 2023;4(3): 100974.
30. Wei L, Xu J, Hu X, Lyu G. Development of a risk model based on immune genes in patients with colon adenocarcinoma. Cancer Rep (Hoboken). 2023;6(2): e1712.
31. Simigdala N, Chalari A, Sklirou AD, Chavdoula E, Papafotiou G, Melissa P, et al. Loss of Kmt2c in vivo leads to EMT, mitochondrial dysfunction and improved response to lapatinib in breast cancer. Cell Mol Life Sci. 2023;80(4):100.
32. Ran FA, Hsu PD, Wright J, Agarwala V, Scott DA, Zhang F. Genome engineering using the CRISPR-Cas9 system. Nat Protoc. 2013;8(11):2281–308.
33. Fuss IJ, Kanof ME, Smith PD, Zola H. Isolation of whole mononuclear cells from peripheral blood and cord blood. Curr Protoc Immunol. 2009;Chapter 7:7 1 -7 1 8.
34. Curtis C, Shah SP, Chin SF, Turashvili G, Rueda OM, Dunning MJ, et al. The genomic and transcriptomic architecture of 2,000 breast tumours reveals novel subgroups. Nature. 2012;486(7403):346–52.
35. Ciriello G, Gatza ML, Beck AH, Wilkerson MD, Rhie SK, Pastore A, et al. Comprehensive Molecular Portraits of Invasive Lobular Breast Cancer. Cell. 2015;163(2):506–19.
36. Berger AC, Korkut A, Kanchi RS, Hegde AM, Lenoir W, Liu W, et al. A Comprehensive Pan-Cancer Molecular Study of Gynecologic and Breast Cancers. Cancer Cell. 2018;33(4):690–705 e9.
37. Cerami E, Gao J, Dogrusoz U, Gross BE, Sumer SO, Aksoy BA, et al. The cBio cancer genomics portal: an open platform for exploring multidimensional cancer genomics data. Cancer Discov. 2012;2(5):401–4.
38. Gao J, Aksoy BA, Dogrusoz U, Dresdner G, Gross B, Sumer SO, et al. Integrative analysis of complex cancer genomics and clinical profiles using the cBioPortal. Sci Signal. 2013;6(269):pl1.
39. de Bruijn I, Kundra R, Mastrogiacomo B, Tran TN, Sikina L, Mazor T, et al. Analysis and Visualization of Longitudinal Genomic and Clinical Data from the AACR Project GENIE Biopharma Collaborative in cBioPortal. Cancer Res. 2023;83(23):3861–7.
40. Aran D, Hu Z, Butte AJ. xCell: digitally portraying the tissue cellular heterogeneity landscape. Genome Biol. 2017;18(1):220.
41. Welsh JA, Goberdhan DCI, O'Driscoll L, Buzas EI, Blenkiron C, Bussolati B, et al. Minimal information for studies of extracellular vesicles (MISEV2023):

From basic to advanced approaches. J Extracell Vesicles. 2024;13(2): e12404.
42. Ge SX, Jung D, Yao R. ShinyGO: a graphical gene-set enrichment tool for animals and plants. Bioinformatics. 2020;36(8):2628–9.
43. Feng M, Cui H, Tu W, Li L, Gao Y, Chen L, et al. An integrated pan-cancer analysis of PSAT1: A potential biomarker for survival and immunotherapy. Front Genet. 2022;13: 975381.
44. Chen J, Wu F, Cao Y, Xing Y, Liu Q, Zhao Z. The novel role of LDHA/LDHB in the prognostic value and tumor-immune infiltration in clear cell renal cell carcinoma. PeerJ. 2023;11: e15749.
45. Frank AC, Raue R, Fuhrmann DC, Sirait-Fischer E, Reuse C, Weigert A, et al. Lactate dehydrogenase B regulates macrophage metabolism in the tumor microenvironment. Theranostics. 2021;11(15):7570–88.
46. Krylova SV, Feng D. The Machinery of Exosomes: Biogenesis, Release, and Uptake. Int J Mol Sci. 2023;24(2).
47. Willms E, Cabanas C, Mager I, Wood MJA, Vader P. Extracellular Vesicle Heterogeneity: Subpopulations, Isolation Techniques, and Diverse Functions in Cancer Progression. Front Immunol. 2018;9:738.
48. Daaboul GG, Gagni P, Benussi L, Bettotti P, Ciani M, Cretich M, et al. Digital Detection of Exosomes by Interferometric Imaging. Sci Rep. 2016;6:37246.
49. Buscher K, Ehinger E, Gupta P, Pramod AB, Wolf D, Tweet G, et al. Natural variation of macrophage activation as disease-relevant phenotype predictive of inflammation and cancer survival. Nat Commun. 2017;8:16041.
50. Agnarelli A, Lauer Betran A, Papakyriakou A, Vella V, Samuels M, Papanastasopoulos P, et al. The Inhibitory Properties of a Novel, Selective LMTK3 Kinase Inhibitor. Int J Mol Sci. 2023;24(1).
51. Cilibrasi C, Ditsiou A, Papakyriakou A, Mavridis G, Eravci M, Stebbing J, et al. LMTK3 inhibition affects microtubule stability. Mol Cancer. 2021;20(1):53.
52. Guerra F, Bucci C. Multiple Roles of the Small GTPase Rab7. Cells. 2016;5(3).
53. Wallace M. Phosphorylation of Rab7 at serine 72 and its role in the regulation of the late endocytic pathway [PhD Thesis]. Cancer Research UK London Research Institute: University College London; 2014.
54. Shinde SR, Maddika S. PTEN modulates EGFR late endocytic trafficking and degradation by dephosphorylating Rab7. Nat Commun. 2016;7:10689.
55. Vanlandingham PA, Ceresa BP. Rab7 regulates late endocytic trafficking downstream of multivesicular body biogenesis and cargo sequestration. J Biol Chem. 2009;284(18):12110–24.
56. Ritter JL, Zhu Z, Thai TC, Mahadevan NR, Mertins P, Knelson EH, et al. Phosphorylation of RAB7 by TBK1/IKKepsilon Regulates Innate Immune Signaling in Triple-Negative Breast Cancer. Cancer Res. 2020;80(1):44–56.
57. Strizova Z, Benesova I, Bartolini R, Novysedlak R, Cecrdlova E, Foley LK, Striz I. M1/M2 macrophages and their overlaps - myth or reality? Clin Sci (Lond). 2023;137(15):1067–93.
58. Bosshart H, Heinzelmann M. THP-1 cells as a model for human monocytes. Ann Transl Med. 2016;4(21):438.
59. Nguyen VVT, Witwer KW, Verhaar MC, Strunk D, van Balkom BWM. Functional assays to assess the therapeutic potential of extracellular vesicles. J Extracell Vesicles. 2020;10(1): e12033.
60. Gupta D, Zickler AM, El Andaloussi S. Dosing extracellular vesicles. Adv Drug Deliv Rev. 2021;178: 113961.
61. Kumarasamy S, Solanki S, Atolagbe OT, Joe B, Birnbaumer L, Vazquez G. Deep Transcriptomic Profiling of M1 Macrophages Lacking Trpc3. Sci Rep. 2017;7:39867.
62. Huang Y, He S, Chen Y, Sheng J, Fu Y, Du X, et al. UCHL1 Promoted Polarization of M1 Macrophages by Regulating the PI3K/AKT Signaling Pathway. J Inflamm Res. 2022;15:735–46.
63. O'Connell PA, Surette AP, Liwski RS, Svenningsson P, Waisman DM. S100A10 regulates plasminogen-dependent macrophage invasion. Blood. 2010;116(7):1136–46.
64. Rodriguez AE, Ducker GS, Billingham LK, Martinez CA, Mainolfi N, Suri V, et al. Serine Metabolism Supports Macrophage IL-1beta Production. Cell Metab. 2019;29(4):1003–11 e4.
65. Cui K, Ardell CL, Podolnikova NP, Yakubenko VP. Distinct Migratory Properties of M1, M2, and Resident Macrophages Are Regulated by alpha(D) beta(2) and alpha(M)beta(2) Integrin-Mediated Adhesion. Front Immunol. 2018;9:2650.
66. Marar C, Starich B, Wirtz D. Extracellular vesicles in immunomodulation and tumor progression. Nat Immunol. 2021;22(5):560–70.
67. Xu D, Chen WQ, Liang MX, Chen X, Liu Z, Fei YJ, et al. Tumor-derived small extracellular vesicles promote breast cancer progression by upregulating PD-L1 expression in macrophages. Cancer Cell Int. 2023;23(1):137.
68. Yanez-Mo M, Siljander PR, Andreu Z, Zavec AB, Borras FE, Buzas EI, et al. Biological properties of extracellular vesicles and their physiological functions. J Extracell Vesicles. 2015;4:27066.
69. Caponnetto F, Manini I, Skrap M, Palmai-Pallag T, Di Loreto C, Beltrami AP, et al. Size-dependent cellular uptake of exosomes. Nanomedicine. 2017;13(3):1011–20.
70. Mathieu M, Nevo N, Jouve M, Valenzuela JI, Maurin M, Verweij FJ, et al. Specificities of exosome versus small ectosome secretion revealed by live intracellular tracking of CD63 and CD9. Nat Commun. 2021;12(1):4389.
71. Liang W, Sagar S, Ravindran R, Najor RH, Quiles JM, Chi L, et al. Mitochondria are secreted in extracellular vesicles when lysosomal function is impaired. Nat Commun. 2023;14(1):5031.
72. Verweij FJ, Bebelman MP, George AE, Couty M, Becot A, Palmulli R, et al. ER membrane contact sites support endosomal small GTPase conversion for exosome secretion. J Cell Biol. 2022;221(12).
73. Patysheva M, Larionova I, Stakheyeva M, Grigoryeva E, Iamshchikov P, Tarabanovskaya N, et al. Effect of Early-Stage Human Breast Carcinoma on Monocyte Programming. Front Oncol. 2021;11: 800235.

## Publisher's Note

Springer Nature remains neutral with regard to jurisdictional claims in published maps and institutional affiliations.